South Virgin–White Hills detachment fault system of SE Nevada and NW Arizona: Applying apatite fission track thermochronology to constrain the tectonic evolution of a major continental detachment fault

Paul G. Fitzgerald,[1] Ernest M. Duebendorfer,[2] James E. Faulds,[3] and Paul O'Sullivan[1,4]

Received 2 August 2007; revised 10 October 2008; accepted 31 October 2008; published 4 March 2009.

[1] The South Virgin–White Hills detachment (SVWHD) in the central Basin and Range province with an along-strike extent of ~60 km is a major continental detachment fault system. Displacement on the SVWHD decreases north to south from ~17 to <6 km. This is accompanied by a change in fault and footwall rock type from mylonite overprinted by cataclasite to chlorite cataclasite and then fault breccia reflecting decreasing fault displacement and footwall exhumation. Apatite fission track (AFT) thermochronology was applied both along-strike and across-strike to assess this displacement gradient. The overall thermal history reflects Laramide cooling (~75 Ma) and then rapid cooling beginning in the late early Miocene. Age patterns reflect some complexity but extension along the SVWHD appears synchronous with rapid cooling initiated at ~17 Ma due to tectonic exhumation. Slip rate is more rapid (~8.6 km/Ma) in the north compared to ~1 km/Ma in the south. The displacement gradient results from penecontemporaneous along-strike motion and formation of the SVWHD by linkage of originally separate fault segments that have differential displacements and hence differential slip rates. East–west transverse structures likely play a role in linkage of different fault segments. The preextension paleogeothermal gradient is well constrained in the Gold Butte block as 18–20°C/km. We present a new thermochronologic approach to constrain fault dip during slip, treating the vertical exhumation rate and the slip as vectors, with the angle between them used to constrain fault dip during slip through the closure temperature of a particular thermochronometer. AFT data from the western rim of the Colorado Plateau constrain the initiation of timing of cooling associated with the Laramide Orogeny at ~75 Ma, and a reheating event in the late Eocene/early Oligocene associated with burial by sediments ("rim gravels") most likely shed from the Kingman High to the west of the plateau. **Citation:** Fitzgerald, P. G., E. M. Duebendorfer, J. E. Faulds, and P. O'Sullivan (2009), South Virgin–White Hills detachment fault system of SE Nevada and NW Arizona: Applying apatite fission track thermochronology to constrain the tectonic evolution of a major continental detachment fault, *Tectonics*, *28*, TC2001, doi:10.1029/2007TC002194.

1. Introduction

[2] The South Virgin–White Hills detachment (SVWHD) is a major continental detachment fault system within the eastern Lake Mead extensional domain of southern Nevada and northwestern Arizona [*Duebendorfer and Sharp*, 1998]. The SVWHD is of importance to geoscientists because it exhibits an along-strike displacement gradient from about 17 km to <6 km over a ~60 km length. Thus by examining the tectonic evolution of this region, including the role that the SVWHD played during profound Miocene extension associated with formation of the central Basin and Range extensional province (terminology of *Wernicke* [1992]), insight will be gained into the along-strike development of detachment fault systems.

[3] At the northern end of the SVWHD, the Gold Butte block has been described as a classic example of a tilted crustal block, exposing ~17 km of crust in the footwall of the Lakeside Mine fault [*Wernicke and Axen*, 1988; *Fryxell et al.*, 1992; *Brady et al.*, 2000]. Previous thermochronology in the Gold Butte block [*Fitzgerald et al.*, 1991; *Reiners et al.*, 2000; *Bernet*, 2002; *Reiners*, 2005] document well the timing of the onset of rapid cooling due to tectonic exhumation, as well as the intact nature of at least the upper ~10 km of the crustal block. However, no thermochronology has been applied to the footwall of the SVWHD to the south of Lake Mead, where the amount of slip on the fault is much less.

[4] In this paper, we integrate new apatite fission track (AFT) thermochronology data from the region south of Lake Mead and the Gold Butte block tilted crustal block with existing thermochronologic and structural data. These data, along with new AFT thermochronology from south of Lake Mead in the footwall of the SVWHD and the abrupt

[1]Department of Earth Sciences, Syracuse University, Syracuse, New York, USA.
[2]Department of Geology, Northern Arizona University, Flagstaff, Arizona, USA.
[3]Nevada Bureau of Mines and Geology, University of Nevada, Reno, New York, USA.
[4]Now at Apatite to Zircon Inc., Moscow, Idaho, USA.

0278-7407/09/2007TC002194

western side of the Colorado Plateau, are evaluated in the context of structural analysis and field observations to address the following questions: (1) Is there a difference in footwall exhumation histories along the strike of the detachment that can be linked to the displacement gradient? (2) If the rate of slip on the SVWHD was the same along its length, can that be explained by a north to south younging for the onset of movement on the SVWHD, or do the slip rates on the detachment vary along-strike, as would be expected if the timing of movement on the fault was synchronous along-strike? (3) What constraints can be placed on the initial dip of the detachment? (4) What is the overall thermal history of the eastern Lake Mead extensional domain, and can we link that to the earlier thermal history derived from the AFT data from the western edge of the Colorado Plateau?

2. Geological Background

[5] The study area in northwestern Arizona and southern Nevada lies in the northern part of the Colorado River extensional corridor [cf. *Faulds et al.*, 2001a] and within the eastern part of the Lake Mead extensional domain [cf. *Spencer and Reynolds*, 1989] (Figure 1a). This region also occupies the easternmost part of the central Basin and Range province of *Wernicke* [1992]. The dominantly east tilted Lake Mead domain includes an area of about 15,000 km^2 and contains two major strike-slip fault systems, the right-lateral Las Vegas Valley shear zone and the left-lateral Lake Mead fault system, both of which are kinematically linked to extension in the region [e.g., *Anderson*, 1973; *Bohannon*, 1984]. Major extension in the Lake Mead domain is bracketed between about 16–9 Ma based on ^{40}Ar/^{39}Ar dates on volcanic units within strongly tilted synextensional sedimentary rocks and angular unconformities with dated, horizontally bedded, postextensional basin fill deposits [e.g., *Anderson*, 1973; *Bohannon*, 1979, 1984; *Beard*, 1996; *Duebendorfer et al.*, 1998]. The magnitude of extension in the Lake Mead domain is less than that in the west tilted Whipple extensional domain to the south, although there is 60–80 km westward transport of the allochthonous Frenchman Mountain block in the Lake Mead region [e.g., *Bohannon*, 1984; *Duebendorfer et al.*, 1998; *Fryxell and Duebendorfer*, 2005]. This transport was accommodated on a combination of normal and strike-slip faults, in comparison to the dominantly normal slip translation in the Whipple domain.

[6] The boundary between the highly extended central Basin and Range province and the generally tectonically stable Colorado Plateau to the east is marked by an abrupt, 800 m high escarpment that corresponds to the west-side-down Grand Wash fault. On the basis of topographic expression, seismic reflection profiles, an abrupt transition from flat-lying unextended strata to moderately to steeply tilted fault blocks, and the geometry of at least three major basins, the Grand Wash fault clearly forms the boundary between the Basin and Range province and the Colorado Plateau in the Lake Mead region [*Lucchitta*, 1972; *Faulds et al.*, 1997; *Brady et al.*, 2000; *Faulds et al.*, 2001b, 2008, 2009]. However, the SVWHD can be considered the dominant structure for much of the extension in the eastern Lake Mead domain, as it probably accommodated much greater normal displacement than the Grand Wash fault zone.

[7] An important feature that occupied the northern Colorado River extensional corridor prior to extension is the Kingman arch [*Bohannon*, 1984], a north plunging structural high from which Paleozoic and Mesozoic sedimentary rocks were eroded primarily as a result of uplift during the Laramide orogeny [*Young and Brennan*, 1974; *Bohannon*, 1984; *Faulds et al.*, 2001a]. This structural high is the northernmost projection of the Mogollon highland that lay south and southwest of the present Colorado Plateau in Arizona. Evidence for the arch in northwest Arizona includes (1) Paleocene and Eocene "rim gravels" deposited at the western and southwestern margins of the Colorado Plateau that were sourced from the west and southwest [*Young and Brennan*, 1974; *Lucchitta*, 1972; *Lucchitta and Young*, 1986] and (2) Miocene strata that lie directly on Proterozoic and Cretaceous crystalline rocks within the northern Colorado River extensional corridor (i.e., postdating erosion of the Paleozoic and Mesozoic section).

3. South Virgin–White Hills Detachment

[8] The broadly north striking, 25–40° west dipping SVWHD (Figures 1a, 1b, 2, and 3) can be traced nearly 60 km south from the Gold Butte area, southern Nevada, to the northern Cerbat Mountains in northwestern Arizona [*Cascadden*, 1991; *Duebendorfer and Sharp*, 1998; *Faulds et al.*, 2001a]. It comprises three low-angle normal faults that accommodated approximately east–west extension. From north to south, these are the Lakeside Mine fault (South Virgin detachment of *Wernicke and Axen* [1988]) in the south Virgin Mountains, the Salt Spring fault in the northern White Hills, and the Cyclopic Mine fault in the southern White Hills [e.g., *Myers et al.*, 1986] (Figure 2). Although it is not possible to establish absolute physical contiguity among these faults because of postextensional sedimentary cover, *Duebendorfer and Sharp* [1998] interpreted them as parts of a single structure because they lie along strike of one another, all have top-to-the-west kinematics, and were active contemporaneously [*Duebendorfer et al.*, 1998]. *Brady et al.* [2000] extended this detachment fault system farther to the north, including the Garden Wash and Gold Butte faults as part of the SVWHD (Figure 4). Displacement on the SVWHD decreases from ~17 km at the Gold Butte block [*Fryxell et al.*, 1992; *Brady et al.*, 2000] in the north to less than 6 km at the Cyclopic Mine in the south [*Price and Faulds*, 1999]. This along-strike, southward decrease in displacement is accompanied by a change in fault and footwall rock type from lower greenschist facies mylonite (i.e., brittle feldspars and unrecovered quartz ribbons), overprinted by cataclasite along the Lakeside Mine fault [*Fryxell et al.*, 1992], to chlorite cataclasite along the Salt Spring fault [*Duebendorfer and Sharp*, 1998], to highly oxidized, locally mineralized fault breccia along the Cyclopic Mine fault [*Myers et al.*, 1986; *Theodore et al.*,

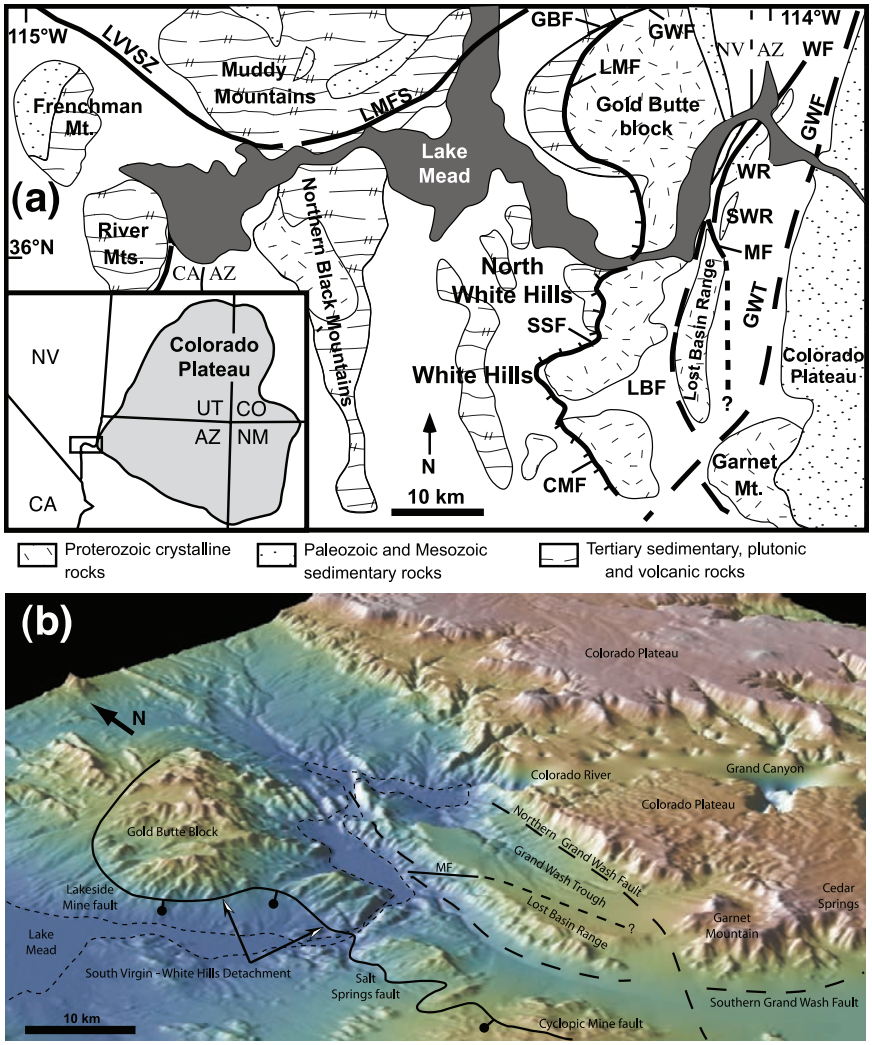

Figure 1. (a) Regional geological map. Faults: CMF, Cyclopic Mine fault; GBF, Gold Butte fault; GWF, Grand Wash fault; LBF, Lost Basin Range fault; LMF, Lakeside Mine fault; LMFS, Lake Mead fault system; LVVSZ, Las Vegas Valley shear zone; MF, Meadview fault (dashed where its likely southerly extension is concealed); SSF, Salt Spring fault; WF, Wheeler Ridge fault. Geographical features: GWT, Grand Wash Trough; SWR, South Wheeler Ridge; WR, Wheeler Ridge. Inset map shows the location of the region (box) with respect to the Colorado Plateau and southwestern states: CA, California; NV, Nevada; AZ, Arizona; NM, New Mexico; CO, Colorado; UT, Utah. (b) Oblique DEM of the SVWHD region. Image is derived using GeoMapApp (http://www.geomapapp.org/). DEM data are from Shuttle Radar Topography Mission (SRTM). Regions appearing "fuzzy," e.g., the Colorado River, reflect smoothed topography generated by the program because of missing data (voids) where the topography is steep.

1987]. The north-to-south transition in fault rock type, from plastic to progressively more brittle, reflects decreasing fault displacement and consequent footwall exhumation from north to south.

[9] The entire footwall of the SVWHD is composed of a heterogeneous suite of Paleo- and Mesoproterozoic crystalline rocks that includes garnet-biotite paragneiss, quartzofeldspathic orthogneiss, amphibolite, and various granitoids. Paleoproterozoic rocks in southern Nevada and northwestern Arizona have been regionally metamorphosed to the granulite facies (i.e., sillimanite-K feldspar ± orthopyroxene in metapelites) [e.g., *Volborth*, 1962; *Young et al.*, 1989; *Fryxell et al.*, 1992; *Duebendorfer et al.*, 2001]. Structurally below the detachment surface proper, in the northern and central parts of the SVWHD, is a zone of greenschist-grade retrogression that ranges in thickness from 50 to more than 150 m. In addition, although highly variable, foliations in the footwall of the SVWHD generally dip less than 30°, mostly to the west, in contrast to the generally steep foliation dips in crystalline rocks throughout

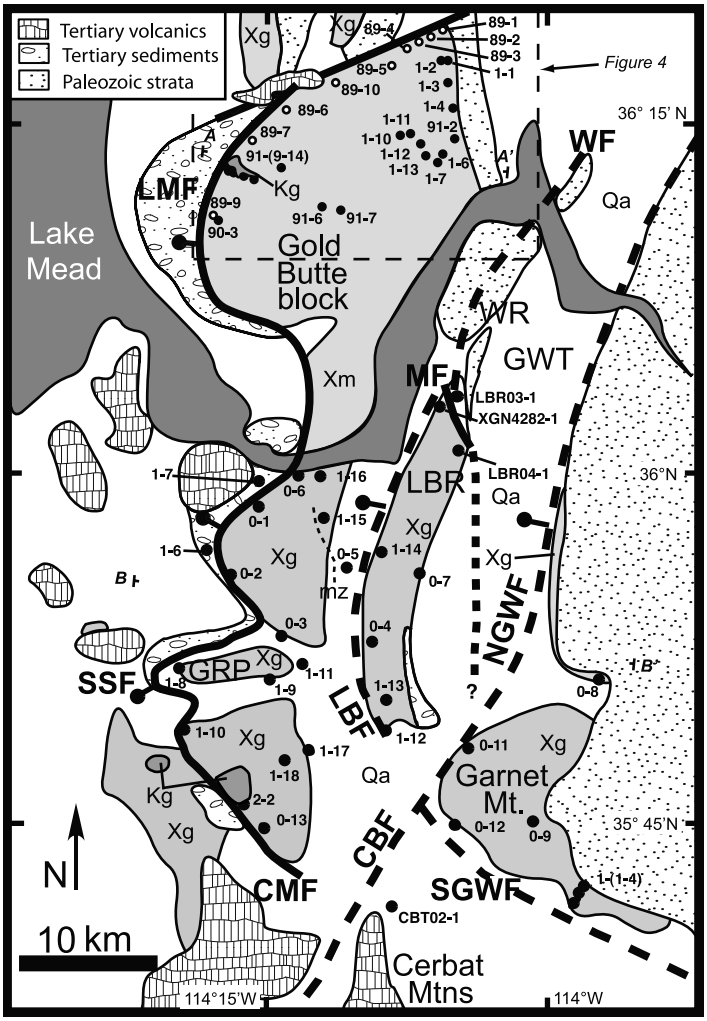

Figure 2. Simplified geological map of the Gold Butte block of southeastern Nevada and White Hills of northwestern Arizona with sample numbers. Geology is after *Fryxell et al.* [1992], *Duebendorfer and Sharp* [1998], and *Brady et al.* [2000]. Abbreviations are as for Figure 1a plus Xg, Proterozoic granite; Xm, Proterozoic metamorphics; Kg, Cretaceous granite; Qa, Quaternary cover; CBF, Cerbat Mountains fault; GRP, Golden Rule Peak; LBR, Lost Basin Range; SGWF, South Grand Wash fault; NGWF, North Grand Wash fault; mz marks the approximate location of the chlorite phyllonite zone in the Hualapai Valley [*Coven*, 2005]. Light gray shade indicates basement rock Xm or Xg. For the Gold Butte block, sample numbers with the prefix 89- are from *Fitzgerald et al.* [1991]; 90-3 is for sample PF90-03; 91-2 is equivalent to sample PF91-02, etc.; 1-1 is equivalent to sample VM01-01, etc. For the White Hills, 0-1 is equivalent to sample WH00-1, etc.; 1-1 is equivalent to sample WH01-1. etc.; and 2-2 is equivalent to sample WH02-2. Also shown are the locations of cross sections for the Gold Butte block (A-A′, Figure 3) and the White Hills (B-B′, Figure 8).

most of northwestern Arizona. The coincidence of low-angle foliation with pervasive retrogression of rocks in the lower plate suggests that tilting of the footwall accompanied motion along the SVWHD.

[10] Hanging wall rocks vary from nonexistent along the Lakeside Mine fault (i.e., they have been tectonically exhumed and are now possibly located at Frenchman Mountain to the west [*Fryxell and Duebendorfer*, 2005]), to east tilted synextensional debris flows and megabreccia deposits along the Salt Spring fault, to a large growth fault basin in the southern White Hills filled with a thick sequence (>3 km) of volcanic and sedimentary rocks [*Price and Faulds*, 1999; *Faulds et al.*, 2001b, 2008, 2009]. On the basis of tilt relations and $^{40}Ar/^{39}Ar$ dates on tuffs (sanidine) and basalts (groundmass concentrates) within synextensional sedimentary sequences, significant extension along the SVWHD occurred between ~16.5 and 14 Ma, with minor extension continuing until about 8 Ma [*Beard*, 1996;

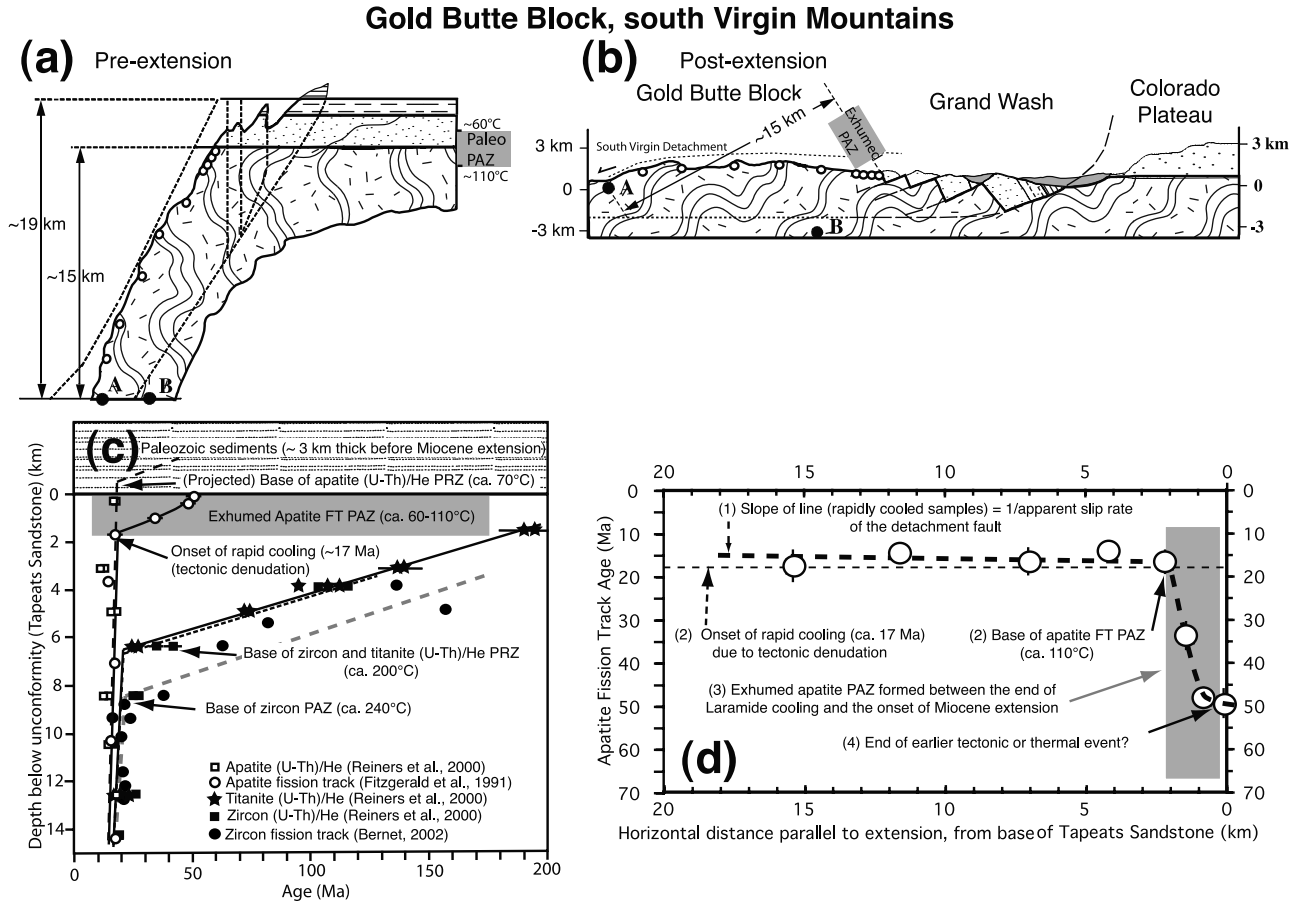

Figure 3. Diagram showing how low-temperature thermochronology can be applied to detachment fault systems. (a) Preextension crustal-scale cross section of the Gold Butte block [after *Wernicke and Axen*, 1988]. Also plotted are the preextension (pretilt) locations for samples from *Fitzgerald et al.* [1991] and the preextension partial annealing zone (PAZ) determined in their study. (b) Present-day crustal cross section of the Gold Butte block [after *Wernicke and Axen*, 1988] with *Fitzgerald et al.* [1991] sample locations and exhumed PAZ. (c) Paleodepth plotted against age for a number of thermochronologic methods. All methods clearly show a break in slope in the profile representing the base of an exhumed PAZ or partial retention zones (PRZ). The break marks the onset of rapid cooling due to tectonic denudation along the Lakeside Mine fault that initiated at ~17 Ma. (d) Apatite fission track (AFT) age for samples from *Fitzgerald et al.* [1991] plotted against horizontal distance (parallel to extension direction) from the unconformity at the base of the Paleozoic section (Tapeats Sandstone). The slope of the line is proportional to the slip rate on the fault [*Foster et al.*, 1993; *Foster and John*, 1999].

Duebendorfer and Sharp, 1998; *Price and Faulds*, 1999; *Faulds et al.*, 2001a; *Blythe*, 2005; *Faulds et al.*, 2008, 2009].

[11] The SVWHD is highly sinuous in map view with kilometer-scale footwall salients marked by topographic highs and footwall reentrants coinciding with topographic lows. Footwall salients are antiformal and reentrants are synformal as indicated by the orientation of cataclastic foliations in the lower plate. This relation between cataclastic foliations and salients/reentrants is particularly striking in the northern White Hills. Superimposed on these macroscopic warps are extension-parallel antiforms and synforms with wavelengths on the order of hundreds of meters to 1000 m (Figure 1b). These smaller features resemble corrugations described from many metamorphic core complexes [*Yin and Dunn*, 1992; *Spencer*, 1999; *Little et al.*, 2007].

4. Apatite Fission Track Thermochronology Applied to Detachment Fault Systems

[12] Low-medium temperature thermochronology is a powerful approach to constraining time-temperature histories of rocks during exhumation from near-surface depths (3–5 km, temperatures of 40–300°C). Common methods include fission track thermochronology, $^{40}Ar/^{39}Ar$ thermo-

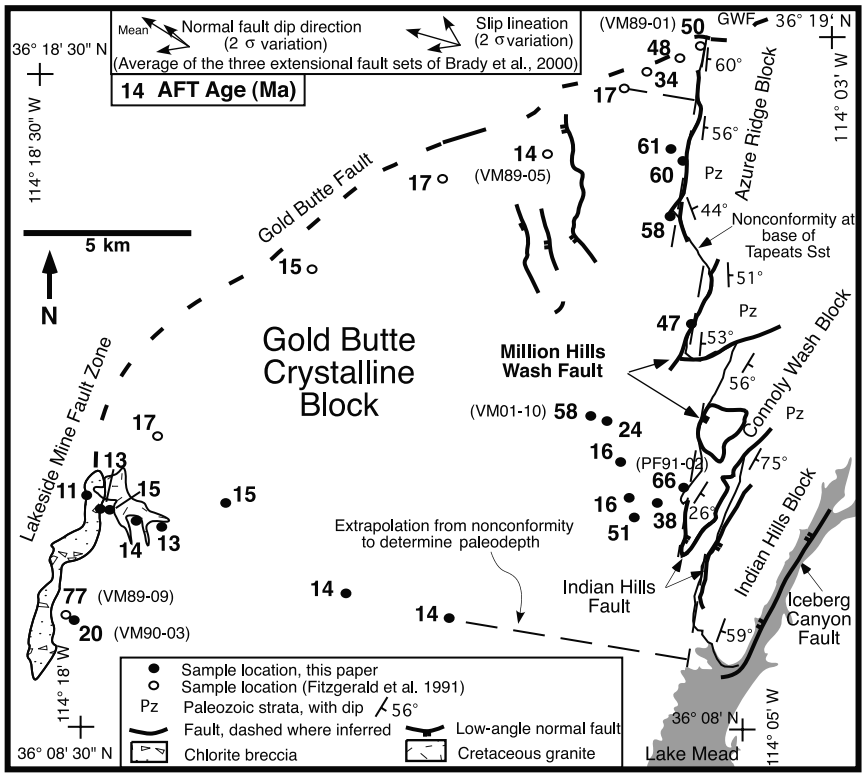

Figure 4. Tectonic sketch map of the Gold Butte block [after *Brady et al.*, 2000] showing AFT ages (Ma) and selected sample names as discussed in the text. GWF, Garden Wash fault. The paleodepth of each sample was determined by measuring the horizontal position from the Paleozoic nonconformity, parallel to the slip direction, and then using a tilt of 56° (the average dip of the Paleozoic sediments on the east side of the Gold Butte) on a planar fault for a rigid block. The Paleozoic strata are disrupted at the eastern end of the block so we calculate paleodepth for each sample as part of one of the four segments, extrapolating perpendicular from the nonconformity.

chronology, and more recently (U-Th)/He dating. All of these methods can be applied to a variety of minerals that provide information on different temperature intervals. However, the most powerful methods are those that incorporate a kinetic parameter that can be used to constrain the rate of cooling, such as $^{40}Ar/^{39}Ar$ thermochronology using potassium feldspar and multidiffusion domain modeling [e.g., *McDougall and Harrison*, 1999] and AFT thermochronology with track length and apatite compositional measurements [e.g., *Ketcham*, 2005]. Use of more than one thermochronometer on the same set of samples will usually provide a more complete record than one method in isolation [e.g., *Reiners et al.*, 2003; *Fitzgerald et al.*, 2006].

[13] Fission track thermochronology has been applied extensively in areas where extensional processes dominate. It has been widely applied in rift flank mountains, including the Red Sea [e.g., *Kohn and Eyal*, 1981], Kenya [e.g., *Foster and Gleadow*, 1996], the Transantarctic Mountains [e.g., *Fitzgerald*, 1994] and the Wasatch Front [e.g., *Naeser et al.*, 1983; *Armstrong et al.*, 2003]. In addition, the concept of the exhumed partial annealing zone (PAZ) was developed from a study in the Transantarctic Mountains [*Gleadow and Fitzgerald*, 1987; *Fitzgerald and Gleadow*, 1990]. Using this concept, the timing and amount of exhumation or denudation can be calculated [*Gleadow and Fitzgerald*, 1987; *Brown*, 1991; *Fitzgerald et al.*, 1995]. If the fission track "stratigraphy" [*Brown*, 1991] of an area is well known, the locations of faults and their displacements [e.g., *Fitzgerald*, 1992; *Foster and Gleadow*, 1996] can also be constrained.

[14] Prior to the application of thermochronologic techniques, relationships between exhumed (and/or tilted) rock units and the regional geology (preextensional, synextensional, and postextensional sedimentary rocks, lava flows, ash deposits, dikes) offered insight into the timing and duration of extension. In the Basin and Range province of the western United States, thermochronological applications have provided important constraints on the timing of extension and rate of slip on detachment faults, as well as constraints on the dip angle of these faults while they were active [e.g., *Fitzgerald et al.*, 1991; *Foster et al.*, 1991, 1993; *John and Foster*, 1993; *Fitzgerald et al.*, 1994; *Howard and Foster*, 1996; *Foster and John*, 1999; *Fayon et al.*, 2000; *Reiners et al.*, 2000; *Stockli et al.*, 2000, 2001, 2002; *Wells et al.*, 2000; *Brady*, 2002; *Reiners*, 2002; *Carter et al.*, 2004, 2006], as summarized by *Stockli* [2005].

Sampling strategy and sample location with respect to controlling structures in studies such as these are essential to providing the tightest constraints on timing of extension and slip rate. In general, the timing of extension and associated footwall exhumation is synchronous with the onset of rapid cooling as recorded by using age-closure temperature graphs for multiple thermochronometers [e.g., *Baldwin et al.*, 1993; *Foster and John*, 1999] or from a single thermochronometer and multiple samples collected over a significant paleodepth. In the latter, the bases of exhumed PAZs (fission track) or partial retention zones (PRZ) ($^{40}Ar/^{39}Ar$ thermochronology or (U-Th)/He dating) indicate the onset of rapid cooling [e.g., *Fitzgerald et al.*, 1991; *Baldwin and Lister*, 1998; *Reiners et al.*, 2000; *Stockli et al.*, 2000, 2002].

[15] In extended terranes, especially in footwalls, an important component of the sampling strategy is to collect samples parallel to the extension direction. The Gold Butte block of southern Nevada is an excellent example of a tilted crustal block that displays multiple exhumed PAZ/PRZs (Figure 3), all indicating the onset of rapid cooling due to extension-related tectonic exhumation at ~17 Ma [*Fitzgerald et al.*, 1991; *Reiners et al.*, 2000]. Note that the paleodepth of each sample is constrained assuming a single planar fault and a rigid block. Should the exhuming fault be listric, the paleodepth calculation will be less for each sample [*Reiners*, 2005]. This will affect the determination of the vertical exhumation rate, and hence angle of the fault during slip, but not the timing of the onset of rapid cooling and hence extension (we discuss this in more detail below). We use the plot of age versus horizontal distance parallel to extension direction for data from *Fitzgerald et al.* [1991] to demonstrate how to interpret such information and to provide a platform for the presentation of the new data. There are four classic components in an age versus horizontal distance diagram (Figure 3d):

[16] 1. Ages from the deepest crustal levels rapidly cooled as a result of tectonic exhumation and slip along the master detachment. Confined fission track lengths have means >14 μm with small standard deviations and ages young progressively toward deeper crustal levels. In general, a regression line will be proportional to the inverse slip rate along the fault. Complications to this simple interpretation (i.e., factors that change the thermal structure in the upper crust) depend on the dip of the fault (the steeper the dip, the greater the underestimate of true slip rate), which thermochronometer is used (higher temperature methods lead to an underestimation of true rate due to more significant advection of isotherms during extension), isostatic rebound of the footwall following tectonic unloading, the effects of syntectonic intrusions, topographic effect on the shape of near-surface isotherms, effects of erosion as well as tectonic exhumation and if there are multiple detachment faults or excisement/incisement of the hanging wall [e.g., *Lister and Baldwin*, 1993; *Ketcham*, 1996; *Foster and John*, 1999; *Stockli*, 2005]. As is the case with using age-elevation profiles to determine apparent exhumation rates, apparent slip rates are averages for the time interval revealed. In the example shown in Figure 3d there are too few samples and the ages overlap such that the apparent slip rate is unconstrained (i.e., infinite). However, if we combine the data of *Fitzgerald et al.* [1991] with the new AFT data presented herein, a more meaningful slip rate is obtained (see below). In general, apparent slip rates in the Colorado River extensional corridor range from ~0.3 cm/a (3 km/Ma) to ~0.9 cm/a [*Foster and John*, 1999].

[17] 2. A break in slope, or inflexion point, marks the base of the apatite PAZ (or PRZ) and indicates the onset of rapid cooling due to tectonic exhumation and the onset of extension. Note that, as is also the case with age-elevation profiles [*Fitzgerald and Gleadow*, 1990], the break in slope slightly underestimates the timing of onset of rapid cooling, as samples that define the base of a PAZ/PRZ still have to cool through the PAZ/PRZ and hence some annealing or age reduction occurs.

[18] 3. A zone of samples that resided for considerable periods of time within a PAZ (or PRZ). These samples are partially annealed, with the rate of annealing (or loss of daughter product due to diffusion) dependent on the sample position within the PAZ. Note that the slope of this section does not indicate an apparent slip rate in the same manner that the slope of an exhumed PAZ (Figure 3c) does not indicate an apparent exhumation rate [*Fitzgerald and Gleadow*, 1990].

[19] 4. At the top of an exhumed PAZ, the variation of age with increasing paleodepth changes from significant (i.e., a gentle slope) to indistinguishable (i.e., a steep slope), representing the change from the period of relative tectonic and thermal stability to an earlier period of more rapid cooling. This component is not recognizable in the AFT data from the Gold Butte block (although we see it in the data from the edge of the Colorado Plateau east of White Hills, see below) or in any of the higher temperature systems such as zircon and titanite (U-Th)/He or zircon fission track ages (Figure 3c). This suggests no significant cooling (or reheating and cooling) effected the entire Gold Butte block since ~200 Ma, including any thermal event associated with the Laramide orogeny. Note that even though two-mica granites at the western end of the block have ages of 64–66 Ma (M. Martin, personal communication as cited by *Reiners et al.* [2000]), all thermochronometer systems for samples close to these granites would have ages of zero during the Cretaceous as they lay well below the base of their respective partial annealing or partial retention zones. *Reiners et al.* [2000] did record a cluster of $^{40}Ar/^{39}Ar$ white mica ages of ~90 Ma in the west central part of the Gold Butte block at a depth of ~14–12 km below the Cambrian nonconformity and interpreted these as evidence of a ~90 Ma cooling event. The reason behind this Cretaceous cooling event remains unclear, but as suggested by *Reiners et al.* [2000], it could have been due to cessation of Sevier thrusting [*Dumitru*, 1990], erosion following the Laramide orogeny [e.g., *Dumitru et al.*, 1994], or regional relaxation of isotherms following intense plutonism in the Sierra Nevada [e.g., *Dumitru et al.*, 1991; *House et al.*, 1997].

[20] As mentioned in component 1, the thermal regime in an active zone of extension is dynamic [*Grasemann and*

Mancktelow, 1993; *ter Voorde and Bertotti*, 1994; *Ehlers and Chapman*, 1999], with the field geotherm being modified owing to the rapidity of extension and the movement of a hot footwall against a cool hanging wall, erosion of the footwall following tectonic exhumation, deposition of sediments on the footwall and any topographic effects on the shape of critical isotherms [*Ehlers et al.*, 2001]. In extended regions, the modification of the field geotherm is most significant following the onset of tectonic exhumation. During rapid slip along a normal fault, isotherms are advected such that critical isotherms in the footwall for the various thermochronologic methods will move toward the surface and the geotherm will increase [e.g., *Ehlers et al.*, 2001]. However, the age of the base of an exhumed PAZ or PRZ, while a slight underestimate, can still constrain the onset of the timing of cooling and exhumation. Nor will advection affect the calculation of the preextension paleogeothermal gradient. However, plots of AFT age versus paleodepth (to determine an exhumation rate) will be an underestimate because of advection [*Ehlers*, 2005] and plots of AFT age versus horizontal distance (to constrain the slip rate) will also underestimate the slip rate [e.g., *Stockli*, 2005]. To determine the slip rate (AFT plotted against horizontal distance on a line parallel to the extension direction), isotherms must be in steady state, near horizontal and stationary [*Ketcham*, 1996; *Foster and John*, 1999]. In areas of rapid extension, isotherms do reach dynamic steady state within ~1 Ma of the initiation of extension [*Ketcham*, 1996].

5. Objectives and Testable Hypotheses

[21] The objectives of applying AFT thermochronology to the Gold Butte block–White Hills region were to track the cooling (i.e., exhumation) history of the footwall of the SVWHD both parallel and normal to the extension direction and thereby to constrain the tectonic evolution of the fault system and the controls on the along-strike displacement gradient. In essence we were seeking to distinguish between two end-member hypotheses: the displacement gradient formed (1) during synchronous along-strike exhumation or (2) during diachronous along-strike exhumation. To determine between these hypotheses, we sampled both along- and across-strike in the footwall of the SVWHD.

[22] Resolution of either of these two end-member hypotheses is important for understanding the spatial and temporal evolution of the SVWHD. It has been widely documented that large normal fault systems grow by linkage of originally separate fault segments [e.g., *Peacock and Sanderson*, 1991, 1994; *Childs et al.*, 1995] rather than by progressive lateral propagation of fault tips of a single rupture [*Anders and Schlische*, 1994; *Schlische and Anders*, 1996]. However, the growth history of a particular normal fault system should be evaluated on a case-by-case basis, especially in the situation of an apparent displacement gradient. Initially, individual normal fault segments grow in length by along-strike propagation of their tips. As tips of adjacent fault segments approach one another during propagation, the two fault segments may merge into a larger fault either by linkage of overlapping or curved en echelon fault segments and/or by the development of new connecting faults [*Peacock and Sanderson*, 1991, 1994; *Ferrill et al.*, 1999]. A result of this growth mechanism is the sinuous map trace that characterizes many high-angle normal faults in the Basin and Range such as the Hurricane (Utah and northern Arizona [*Stewart and Taylor*, 1996]), Wasatch (Utah [*Armstrong et al.*, 2004]), Beaverhead (Idaho [*Anders and Schlische*, 1994]) faults, and the 1915 Pleasant Valley earthquake rupture (Nevada [*Wallace*, 1984; *dePolo et al.*, 1991]). This sinuous map trace can be accentuated by footwall tilting to produce the extension-parallel corrugations observed in many low-angle normal fault systems [*Ferrill et al.*, 1999].

[23] AFT thermochronology can be a useful tool for distinguishing between the two fault-growth models referred to above because the two end-member hypotheses predict different footwall age progressions resulting from fault motion and associated footwall exhumation. For example, growth and development of the SVWHD by linkage of originally separate normal fault segments would likely result in synchronous along-strike exhumation (hypothesis 1 above), with individual segments initiating at approximately the same time followed by linkage into a master fault system. Whether or not this predicted consequence of the fault linkage model could be resolved by AFT data would depend on the overall rate of fault growth. If fault growth by linkage were rapid, it is unlikely that AFT could resolve the timing difference in exhumation between the original, early formed fault segments and their younger regions of linkage. Regardless, the fault linkage model predicts approximately coeval exhumation, and therefore similar AFT ages on footwall rocks, along the entire length of the detachment.

[24] If there were approximately synchronous exhumation (hypothesis 1), the difference in displacement magnitude (from north to south in the case of the SVWHD) should result from differential slip rates, i.e., nearly simultaneous exhumation, but at different rates along strike. The measured slip rate (e.g., Figure 3d) would decrease to the south and the north-to-south decrease in footwall exhumation (due to decreased displacement to the south) would be manifested by a southward increase in AFT ages along the SVWHD, with older ages indicating less exhumation. In addition, for hypothesis 1 to be correct, the pattern of ages in west–east transects collected across-strike (e.g., Figures 3c and 3d) would reveal simultaneous initiation of rapid cooling associated with extension, and that the "break in slope" (the base of the exhumed PAZ) would be the same age everywhere in the footwall and not lie parallel to the SVWHD but trend closer to the detachment fault due to decreased displacement to the south.

[25] Progressive lateral propagation of a single rupture, as in hypothesis 2 above, would predict older (i.e., earlier exhumation) AFT ages in the footwall of the areas of highest displacement along the fault, which may be near the center of the final fault [*Watterson*, 1986; *Walsh and Watterson*, 1988; *Cowie and Scholz*, 1992]. Unless propagation was relatively rapid, AFT footwall ages should become progressively younger toward the tips of the final

fault. Hypothesis 2 should also yield a broader range of AFT ages because the total distance of propagation of the two fault tips would far exceed the relatively small distance of propagation necessary for linkage of a number of smaller original fault segments. If hypothesis 2, (diachronous exhumation) is correct, then the displacement gradient is related to the temporal evolution of the fault (i.e., fault growth by north-to-south, south-to-north, or from both directions out from a central location, or some other more complex configuration). In addition, it is expected that the pattern of ages in west–east transects collected across-strike (e.g. Figures 3c and 3d) would reveal diachronous initiation of rapid cooling associated with extension. Whether or not the base of the exhumed PAZ trended closer to the SVWHD or was subparallel to the SVWHD would depend on the relative displacement vectors: north–south initiation of slip versus west–east slip rate.

[26] Each hypothesis thus has different implications for the model(s) of normal fault evolution applicable to northwestern Arizona. Distinction between these two end-member hypotheses requires the following:

[27] 1. The variation of AFT ages is sufficient to resolve differences in timing of exhumation, which is not always the case given the rapidity of cooling for samples collected in the footwall of normal faults. However, track length information does permit the distinction between rapidly and slowly cooled samples and hence facilitates the identification of exhumed PAZs and the time of initiation of rapid cooling due to tectonic exhumation resulting from extension.

[28] 2. There is enough "crust" exposed east of the Salt Spring and Cyclopic Mine faults in the White Hills to reveal the base of an exhumed PAZ and hence constrain the timing for the onset of extension, as well as constrain slip rates.

[29] 3. Faults such as the Lost Basin Range fault and the Wheeler Ridge faults (Figure 1) do not complicate the age pattern and prevent distinguishing between the two hypotheses. However, one of the advantages of AFT thermochronology is that reliable ages can often be obtained in rocks that are deformed, altered, and faulted, such as those in the footwall near the SVWHD, which could not normally be dated by other isotopic techniques. On the other hand, the relatively lower precision of the AFT technique in comparison to other relatively higher precision techniques does not permit the variation in slip rate to be well constrained [e.g., *Carter et al.*, 2004, 2006].

6. Gold Butte Block: Results and Discussion

[30] In order to fully understand the along-strike development of this detachment fault system, we separately assess the thermochronologic and tectonic evolution of the Gold Butte block, where our new data add to the existing data from multiple methods, and the White Hills area. On the eastern side of the Gold Butte block, AFT ages tend to be older (>17 Ma) and have track length distributions (means $\leq$13 μm, standard deviations $\geq$1.8 μm) indicative of a more complex thermal history and residence within an apatite PAZ before later rapid cooling (Figure 4 and Table 1). In contrast, AFT ages on the western side of the block yield AFT ages $\leq$17 Ma with track length distributions (means >14 μm, standard deviations $\leq$1.8 μm) indicative of rapid cooling. A plot of the new and existing AFT data shows the initiation of rapid cooling in the Miocene at $\sim$17 Ma (see section 6.1 and Figure 5a). Plotting the new AFT ages plus existing data versus horizontal distance parallel to the slip direction allows us to constrain the slip rate (see section 6.2). These new AFT data confirm the original interpretations of *Fitzgerald et al.* [1991] and *Reiners et al.* [2000], with slight modification.

[31] Prior to further discussion of the data, a discussion of sample paleodepth determination is warranted. Sample depth was determined assuming uniform tilting on a planar fault across the Gold Butte block and a horizontal attitude for the Tapeats Sandstone (average dip now $\sim$56° to the east) prior to extension [*Wernicke and Axen*, 1988]. To determine relative sample position, we projected data points along a line parallel to the extension direction and approximately perpendicular to the strike of the Tapeats Sandstone. The strike of the Tapeats Sandstone is somewhat disrupted because of faulting in the Paleozoic strata [*Brady et al.*, 2000] but can be divided into four segments (Figure 4). Sample elevation as well as the en echelon offset of the Paleozoic section was taken into account when determining sample distance from the nonconformity and paleodepth. Folding (a 5° east dipping reverse drag rollover monocline) of Pliocene and Pleistocene deposits on the hanging wall block of the Wheeler Ridge fault [*Howard et al.*, 2000] extrapolated north into the Gold Butte block is likely responsible for part of the dip of the Paleozoic units on the east side of the block. This would decrease the tilt of the Gold Butte block due to Miocene extension and hence the estimate for the thickness of the Gold Butte crustal exposure. We do not correct for this possible $\sim$5° post-early Pliocene tilt, as given the variation in the dip of strata (from $\sim$30° to near vertical), to obtain an average of $\sim$56° any additional minor correction would be within paleodepth estimates for the samples. *Reiners et al.* [2000] used a dip of 65° to determine paleodepth of the samples. In addition (as discussed below) there appears to be disruption and some crustal duplication within the Proterozoic basement in the upper (eastern) part of the Gold Butte block as shown by these new AFT ages.

6.1. Timing of Extension

[32] The pattern of AFT ages plotted versus paleodepth indicates that the onset of rapid cooling began $\sim$17 Ma. Samples with AFT ages older than $\sim$17 Ma spent considerable residence time within an apatite PAZ, while samples with AFT ages $<\sim$17 Ma cooled rapidly through the apatite PAZ. The timing for the onset of rapid cooling is also shown by a plot of AFT age versus mean length (Figure 6). Thus, the interpretation remains the same as described by *Fitzgerald et al.* [1991]. The dramatic break in slope in the age-paleodepth profile (Figure 5a) at $\sim$1.6 km below the nonconformity represents the base of an exhumed PAZ and marks the onset of rapid cooling due to tectonic exhumation. Exhumed PRZs are also revealed in zircon and titanite (U-Th)/He age versus paleodepth and the zircon fission track versus paleodepth profiles (Figure 3c) from the Gold Butte block

Table 1. Fission Track Analytical Results: Gold Butte Block of Southeastern Nevada and White Hills of Northwest Arizona[a]

Sample	Locality	Lat, Long	Elevation (m)	Rock Type	Number of Grains	Standard Track Density (10^6 cm^{-2})	Fossil Track Density (10^5 cm^{-2})	Induced Track Density (10^6 cm^{-2})	Chi-Square Probability (%)	Relative Error (%)	Central Age	Mean Track Length* (μm)	SD (μm)
Gold Butte Block (South Virgin Mountains, SE Nevada)													
VM90-03	VM89-09 locality Chloritic breccia	N36°10.29′, W 114°18.17′	728	Chlorite breccia	7	1.66 (4365)	1.805 (28)	2.669 (414)	77	0.7	20.2 ± 4.0		
PF91-02	East of Cottonwood Wash	N 36° 12.08′, W 114°6.21′	951	Garnet gneiss	25	0.8006 (2598)	3.322 (483)	0.7346 (1068)	78	0.9	65.5 ± 4.0	12.8 ± 0.2 (120)	1.8
PF91-06	Twin Springs	N 36° 10.57′, W 114°12.84′	1065	Garnet gneiss	25	0.8006 (2598)	0.8057 (112)	0.8639 (1201)	74	10	13.7 ± 1.4	14.6 ± 0.1 (100)	1.1
PF91-07	East end of Jumbo Basin	N 36° 10.14′, W 114°10.86′	1210	Orthogneiss	25	0.8006 (2598)	1.171 (163)	1.203 (1674)	95	1	14.2 ± 1.2	14.4 ± 0.1 (110)	1.2
PF91-09	Twin Springs Wash	N 36° 12.23′, W 114°17.91′	705	Chlorite breccia	25	0.8006 (2598)	0.2127 (27)	0.2757 (350)	90	<0.1	11.2 ± 2.2	14.3 ± 0.2 (56)	1.0
PF91-10	Twin Springs Wash	N 36° 12.03′, W 114°17.61′	710	Garnet gneiss (PR)	21	0.8006 (2598)	1.065 (107)	1.231 (1237)	77	4	12.6 ± 1.3	14.4 ± 0.3 (18)	0.9
PF91-11	Twin Springs Wash	N 36° 12.03′, W 114°17.43′	735	Two-mica granite	25	0.8062 (2616)	1.091 (122)	1.063 (1189)	86	0.2	15.0 ± 1.5	14.3 ± 0.2 (39)	1.8
PF91-12	Twin Springs Wash	N 36° 11.82′, W 114°16.91′	790	Garnet gneiss (CR)	25	0.8062 (2616)	0.3543 (43)	0.3643 (440)	100	0	14.3 ± 2.3	14.4 ± 0.3 (20)	1.2
PF91-13	Twin Springs - Rattlesnake Wash	N 36° 11.72′, W 114° 16.43′	810	Two-mica granite	25	0.8062 (2616)	0.08183 (13)	0.09504 (151)	96	<0.1	12.6 ± 3.7	14.3 ± 0.3 (9)	0.7
PF91-14	Rattlesnake Wash	N 36° 12.06′ W 114° 15.17′	900	Garnet gneiss (PR)	25	0.8062 (2616)	0.4396 (61)	0.4447 (617)	95	<0.1	14.5 ± 2.0	14.1 ± 0.2 (55)	1.0
VM01-01	Azure Ridge	N 36° 17.26′ W 114° 06.04′	1170	Granite	25	1.414 (4742)	9.340 (1125)	3.987 (4803)	7	12	60.1 ± 2.7	11.8 ± 0.2 (105)	1.9
VM01-02	Immigrant Canyon	N 36° 17.47′ W 114° 06.27′	1128	Garnet Gneiss	11	1.419 (4742)	4.610 (76)	1.929 (318)	100	0	61.3 ± 7.9	12.0 ± 0.2 (50)	2.1
VM01-03	Indian Trail	N 36° 16.39′ W 114° 06.33′	1341	Garnet -mica gneiss	13	1.424 (4742)	4.453 (176)	1.966 (777)	72	0	58.4 ± 4.9	11.5 ± 0.4 (16)	1.9
VM01-04	South of Connoly Spring at pass	N 36° 14.66′ W 114° 05.96′	1040	Granite gneiss	11	1.435 (4742)	4.516 (102)	2.506 (566)	99	0	46.9 ± 5.1	12.3 ± 0.3 (21)	2.2
VM01-06	Cottonwood Wash	N 36° 11.91′ W 114° 06.75′	760	Garnet gneiss	25	1.456 (4742)	4.421 (598)	3.052 (4128)	33	3	38.3 ± 1.8	11.3 ± 0.2 (130)	2.6
VM01-07	Cottonwood Canyon - mouth	N 36° 11.66′ W 114° 07.21′	710	Rapakivi granite	8	1.461 (4742)	5.20 (82)	2.701 (426)	84	<0.1	50.9 ± 6.2	11.6 ± 0.3 (13)	2.3
VM01-10	Cottonwood Canyon Road	N 36° 13.28′ W 114° 08.0′	1110	Rapakivi granite	25	1.482 (4742)	0.3384 (34)	0.1563 (157)	100	0	58.1 ± 11.0	11.3 ± 0.3 (34)	1.9
VM01-11	Cottonwood Canyon Road	N 36° 13.18′ W 114° 07.69′	975	Rapakivi granite	26	1.492 (4742)	1.707 (206)	1.938 (2339)	3	29	24.8 ± 2.4	13.0 ± 0.2 (101)	2.3
VM01-12	Cottonwood Canyon Road	N 36° 12.52′ W 114° 07.46′	902	Rapakivi granite	25	1.498 (4742)	2.019 (76)	3.422 (1288)	99	0	16.0 ± 1.9	14.3 ± 0.1 (100)	1.2
VM01-13	Cottonwood Canyon Road	N 36° 11.96′ W 114° 07.29′	780	Rapakivi granite	25	1.503 (4742)	0.9172 (75)	1.719 (1406)	9	32	16.0 ± 2.4	14.4 ± 0.2 (84)	1.1
White Hills, NW Arizona													
WH00-1	Salt Spring Wash	N 35° 58.900′ W 114° 15.552′	524	Bio-qtz-fsp gneiss	25	1.40 (4471)	1.382 (137)	2.663 (2641)	67	<1	13.2 ± 1.2	13.6 ± 0.2 (76)	1.0
WH00-2	Salt Spring Wash	N 35° 56.645′ W 114° 16.129′	698	Qtz-fsp gneiss, (alteration)	16	1.40 (4471)	0.6485 (50)	1.316 (1015)	50	4	12.6 ± 1.8	14.6 ± 0.1 (11)	1.1

Table 1. (continued)

Sample	Locality	Lat, Long	Elevation (m)	Rock Type	Number of Grains	Standard Track Density (10^6 cm^{-2})	Fossil Track Density (10^5 cm^{-2})	Induced Track Density (10^6 cm^{-2})	Chi-Square Probability (%)	Relative Error (%)	Central Age	Mean Track Length* (μm)	SD (μm)
WH00-3	Between Hualapai and Salt Springs Washes	N 35° 54.690′ W 114° 13.385′	823	Mig gt-bio gneiss	25	1.41 (4471)	0.9016 (99)	1.32 (1450)	72	<1	17.5 ± 1.8	14.2 ± 0.1 (92)	1.0
WH00-4	East side of Hualapai Wash	N 35° 54.456′ W 114° 09.097′	853	Bio-qtz-fsp gneiss	28	1.38 (4738)	0.3796 (68)	0.5974 (1070)	76	<1	15.9 ± 2.0	14.0 ± 0.2 (74)	1.4
WH00-5	West side of Hualapai Wash	N 35° 56.369′ W 114° 09.860′	622	Mig. bio gneiss	26	1.398 (4738)	0.8358 (124)	1.416 (2101)	28	26	14.9 ± 1.7	13.8 ± 0.1 (54)	1.1
WH00-6	Greggs Hideout, Lake Mead - south shore	N 35° 59.645′ W 114° 13.312′	488	Bio-granite	25	1.42 (4738)	0.5722 (82)	0.9505 (1362)	85	3	15.5 ± 1.8	13.5 ± 0.3 (24)	1.5
WH00-7	Climax Mine, Lost Basin Range	N 35° 56.489′ W 114° 06.674′	1170	Fol. granite, (alteration)	26	1.43 (4738)	0.4058 (59)	0.5861 (852)	7	23	19.5 ± 2.9	13.8 ± 0.1 (61)	1.1
WH00-8	Quarry south of Grapevine Wash	N 35° 53.036′ W 114° 00.534′	1219	Bio-granite	26	1.44 (4738)	9.967 (1383)	2.85 (3954)	36	6	90.8 ± 3.4	11.9 ± 0.2 (125)	2.6
WH00-9	Above SE corner of Iron Spring Basin	N 35° 48.208′ W 114° 00.388′	1875	Bio-granite	25	1.45 (4738)	11.57 (1574)	3.25 (4421)	14	9	93.2 ± 3.6	11.7 ± 0.2 (143)	2.4
WH00-11	Southern Grapewine Mesa	N 35° 51.234′ W 114° 03.605′	1317	Granite (alteration)	25	1.47 (4738)	3.055 (456)	1.187 (1772)	72	<1	68.2 ± 3.7	13.2 ± 0.2 (110)	1.5
WH00-12	Base of SW ridge of Garnet Mtn	N 35° 47.552′ W 114° 05.440′	1006	Fol. bio-granite	20	1.48 (4738)	16.45 (1486)	6.784 (6129)	44	1	64.8 ± 2.1	12.5 ± 0.1 (130)	1.6
WH00-13	Near Cyclopic Mine, southern White Hills	N 35° 46.739′ W 114° 14.389′	1298	Bio granite	25	1.49 (4738)	1.834 (77)	3.11 (1306)	99	<1	15.9 ± 1.9	13.9 ± 0.2 (64)	1.2
WH01-1	Grand Wash Cliffs, Cedar Springs	N 35° 46.442′ W 113° 57.688′	1573	Granite (alteration)	25	1.55 (5012)	3.524 (504)	0.896 (1282)	99	<1	109.5 ± 6.0	12.5 ± 0.2 (100)	2.2
WH01-2	Grand Wash Cliffs, Cedar Springs	N 35° 46.634′ W 113° 57.870′	1448	Granite (alteration)	25	1.55 (5012)	12.35 (1494)	3.834 (4638)	23	14	89.8 ± 4.1	12.1 ± 0.2 (110)	2.1
WH01-3	Grand Wash Cliffs, Cedar Springs	N 35° 46.478′ W 113° 58.799′	1341	Bio-granite	25	1.55 (5012)	13.14 (1709)	4.609 (5994)	81	<1	79.6 ± 2.5	12.3 ± 0.2 (120)	1.9
WH01-4	Grand Wash Cliffs, Cedar Springs	N 35° 45.523′ W 113° 59.768′	1149	Grey granite	25	1.55 (5012)	14.39 (1758)	5.225 (6382)	1	13	73.6 ± 3.2	12.4 ± 0.2 (116)	2.0
WH01-6	Salt Spring Wash	N 35° 57.558′ W 114° 15.863′	623	Granite gneiss	25	1.55 (5012)	2.554 (286)	3.096 (3480)	77	<1	23.0 ± 1.5	14.1 ± 0.2 (40)	1.4
WH01-7	Salt Spring Wash	N 35° 59.193′ W 114° 15.651′	463	Rhylolitic tuff in megabreccia	25	1.55 (5012)	0.967 (137)	1.438 (2036)	97	<1	18.9 ± 1.7	14.5 ± 0.2 (65)	1.2
WH01-8	West end of Golden Peak Range	N 35° 53.862′ W 114° 17.201′	945	Megacrystic granite	19	1.55 (5012)	1.715 (56)	3.630 (1185)	100	0	13.3 ± 1.8	14.4 ± 0.3 (11)	0.9
WH01-9	Golden Rule Peak	N 35° 53.158′ W 114° 14.440′	1012	Mig gneiss	25	1.55 (5012)	1.650 (101)	2.730 (1671)	94	<1	17.0 ± 1.8	14.3 ± 0.2 (41)	1.2
WH01-10	White Elephant Wash, south side	N 35° 51.656′ W 114° 14.975′	1036	Gneiss	25	1.55 (5012)	2.380 (110)	4.120 (1904)	99	<1	16.2 ± 1.6	14.0 ± 0.2 (26)	1.0
WH01-11	East end of Golden Rule Range	N 35° 53.631′ W 114° 12.760′	841	Gneiss	25	1.55 (5012)	1.722 (118)	2.708 (1856)	98	0	17.8 ± 1.7	14.1 ± 0.2 (25)	0.9
WH01-12	South end of Lost Basin Range	N 35° 50.459′ W 114° 07.570′	975	Gneiss	18	1.55 (5012)	0.659 (71)	1.208 (1301)	84	<1	15.3 ± 1.9	14.4 ± 0.4 (20)	1.5

Table 1. (continued)

Sample	Locality	Lat, Long	Elevation (m)	Rock Type	Number of Grains	Standard Track Density (10^6 cm^{-2})	Fossil Track Density (10^5 cm^{-2})	Induced Track Density (10^6 cm^{-2})	Chi-Square Probability (%)	Relative Error (%)	Central Age	Mean Track Length* (μm)	SD (μm)
WH01-13	Lost Basin Range, pass near south end	N 35° 51.756′ W 114° 08.090′	951	Diorite	25	1.55 (5012)	1.185 (152)	2.046 (2624)	54	13	16.3 ± 1.5	14.3 ± 0.2 (57)	1.1
WH01-14	Golden Gate Mine	N 35° 57.033′ W 114° 07.941′	817	Qtz-rich gneiss	25	1.55 (5012)	0.3669 (50)	0.5195 (708)	100	0	19.8 ± 2.9	14.7 ± 0.3 (12)	1.2
WH01-15	Road to Lake Mead	N 35° 57.952′ W 114° 10.973′	625	Granite gneiss	25	1.55 (5012)	1.043 (157)	1.981 (2983)	42	18	15.1 ± 1.4	13.4 ± 0.2 (58)	1.6
WH01-16	4WD road to Spring Canyon	N 35° 59.705′ W 114° 11.433′	524	gt gneiss	17	1.55 (5012)	1.655 (128)	2.505 (1938)	83	<1	18.5 ± 1.7	13.2 ± 0.2 (44)	1.6
WH01-17	South of White Elephant Wash	N 35° 49.370′ W 114° 11.353′	988	Granite gneiss	25	1.55 (5012)	0.3881 (53)	0.580 (792)	88	<1	18.8 ± 2.7	13.5 ± 0.2 (68)	1.6
WH01-18	South of White Elephant Wash	N 35° 49.073′ W 114° 13.732′	1134	Granite gneiss	25	1.55 (5012)	0.1913 (18)	0.3177 (299)	97	<1	16.9 ± 4.1	14.0 ± 0.2 (32)	1.3
WH02-2	Foot wall of Cyclopic Fault	N 35° 48.517′ W 114° 15.200′	1348	Two mica granite	25	1.336 (2544)	0.178 (376)	0.334 (2320)	55	0	12.8 ± 3.0	14.5 ± 0.2 (18)	0.9
CBT02-1	North Cerbat Mountains	N 35° 43.643′ W 114° 07.416′	890	Lin granite gneiss	25	1.328 (2544)	10.741 (1173)	3.499 (3821)	22	8	73.0 ± 3.1	12.2 ± 0.2 (133)	1.9
XGN4282-1	Northern Lost Basin Range	N 36° 02.764′ W 114° 06.635′	459	Bio-qtz-fsp gneiss	25	1.313 (2544)	2.11 (253)	3.302 (3959)	12	16	15.3 ± 1.2	14.6 ± 0.1 (101)	1.4
LBR04-1	Northern Lost Basin Range	N 35° 59.972′ W 114° 05.662′	933	Bio-qtz-fsp gneiss	2	1.60 (3677)	0.907 (7)	1.347 (120)	41	0	19.4 ± 7.6		

Sample	Locality	Lat, Long	Elevation (m)	Rock Type	Number of Grains	Area Analyzed (cm^2)	ξ_{MS}	^{43}Ca bkg:sig	^{238}U bkg:sig	Chi-Square Probability (%)	Central Age	Mean Track Length* (μm)	SD (μm)
LBR03-1	Lost Basin Range	36° 2.885′ N, W 114° 05.656′	541	amphibolite	22	8.43E-4	11.82	3.7E-2	8.6E-2	1.9	126.6 ± 8	13.5 ± 0.2 (106)	1.7

[a]Parentheses enclose number of tracks counted (density) or measured (track lengths). Standard and induced track densities were measured on mica external detectors (geometry factor of 0.5), and fossil track densities were measured on internal mineral surfaces. Samples of basement rock were crushed and the apatites were separated using conventional heavy liquid and magnetic techniques. Apatites were mounted in epoxy resin on glass slides, ground and polished to reveal an internal surface, and then etched for 20 s at room temperature in 5N HNO_3 to reveal spontaneous fission tracks. All but one of the apatite ages were determined using the external detector method and an automated stage. Mica detector samples were irradiated at the Oregon State University Nuclear Reactor in the slow soaker position B-3 (thermal column 5) that has a Cd for Au ratio of 13.6 at the column face. The mounts were counted at a magnification of 1250X under a dry 100X objective. Ages were calculated using the zeta calibration method using the standard glass CN5 by PGF (zeta = 361 ± 5) and POS (363.5 ± 5) following the procedures of *Hurford and Green* [1983] and *Green* [1985]. Analytical errors were calculated using the ''conventional method'' [*Green*, 1981]. The chi-square test performed on single-grain data [*Galbraith*, 1981] determines the probability that the counted grains belong to a single age population (within Poissonian variation). If the chi-square value is less than 5%, it is likely that the grains counted represent a mixed-age population with real age differences between single grains. The relative error or age dispersion (spread of the individual grain data) is given by the relative standard deviation of the central age. Where the dispersion is low (<15), the data are consistent with a single population, and the mean/pooled ages and the central age converge. Track lengths were measured using ''confined'' fossil fission tracks using only those that were horizontal [*Laslett et al.*, 1984]. Wherever possible, 100 track lengths per sample were measured, the number being less only when insufficient suitable tracks were present in the available apatite. Sample LBR03-1 was processed using the LA-ICP-MS method (using a beam width of 16 μm) following the procedures outlined by *Donelick et al.* [2005]. The apatite age was determined using the LA-ICP-MS zeta calibration factor (ξ_{MS}) determined for each sample by analyzing the U:Ca ratio (for apatite) of grains from an apatite calibration standard with known age (e.g., Durango apatite, 30.6 ± 0.3 Ma from Cerro de Mercado, Durango, Mexico) at the beginning and end of each session on the LA-ICP-MS [*Donelick et al.*, 2005]; bkg:sig, the background to signal ratio in terms of count rate from the LA-ICP-MS; qtz, quartz; fsp, feldspar; bio, biotite; Mig, migmatite; gt, garnet; Fol, foliated; Lin, lineated.

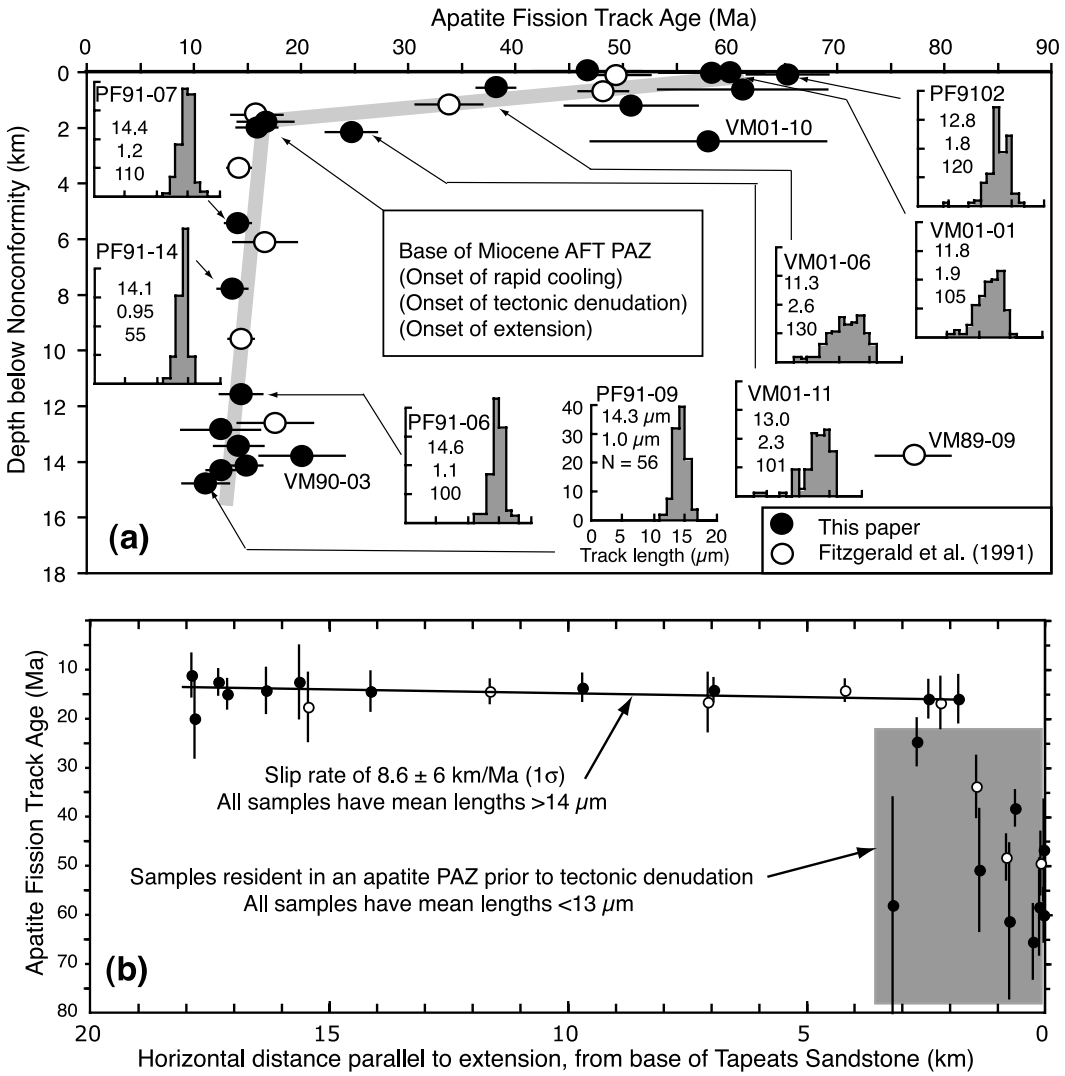

Figure 5. (a) AFT age versus paleodepth. The distinctive break in slope at a paleodepth ~1.6 km below the sub-Cambrian unconformity represents the base of an exhumed PAZ, ~110°C prior to the onset of rapid cooling at ~17 Ma due to tectonic denudation as a result of extension and tilting of the Gold Butte block. Selected confined track length distributions are shown; for example, PF91-07 has a mean length of 14.4 μm and a standard deviation of 1.2 μm, and 110 tracks were measured. Note the classic track length distributions of an exhumed PAZ: samples above the break in slope resided in a PAZ for considerable periods as indicated by mean lengths typically $\leq$13 μm and standard deviations typically $\geq$2 μm. Samples that lie off the trend are labeled (VM01-10, VM90-03, VM89-09) and discussed in the text. (b) AFT age for samples plotted against horizontal distance (parallel to extension direction) from the nonconformity at the base of the Paleozoic section (Tapeats Sandstone). The slope of the line for rapidly cooled samples is proportional to the slip rate on the fault, 8.6 ± 6 km/Ma.

[*Reiners et al.*, 2000; *Bernet*, 2002; *Reiners*, 2005]. The bases of these exhumed PRZs also indicate that the onset of rapid cooling due to tectonic exhumation was initiated ~17 Ma.

6.2. Coherence of the Gold Butte Block

[33] In simple balanced reconstructions, the Gold Butte block has been portrayed as a single crustal block [*Wernicke and Axen*, 1988; *Fryxell et al.*, 1992]. While simplistic, this synopsis is verified by the previous thermochronology results (Figure 3c) that do not show any major disruption to the simple age-paleodepth relationships. If there was major faulting within the Gold Butte block it should be revealed by offset of ages (AFT, zircon and titanite (U-Th)/He, zircon FT) on the gentle slope (for samples lying above the base of an exhumed PAZ or PRZ) of the age-paleodepth

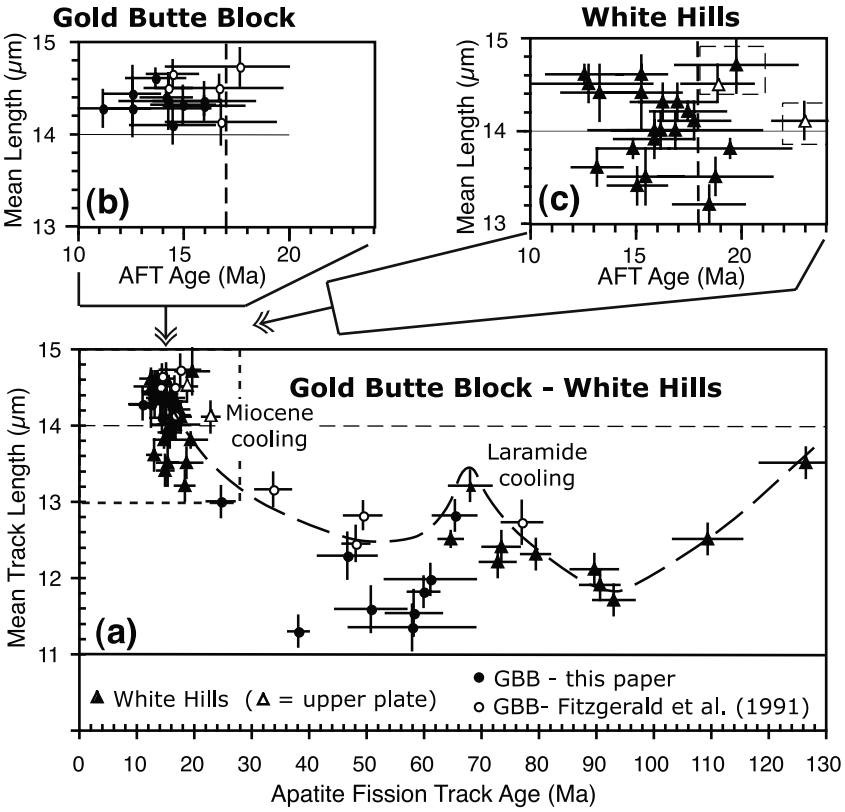

Figure 6. (a) Mean track length plotted against AFT age for all samples from the Gold Butte block and the White Hills. (b) Enlargement of the plot for Gold Butte block samples with an AFT age <24 Ma. Basically, samples with mean lengths >14 μm indicate rapid cooling due to tectonic exhumation. It is clear from this plot, taking into account errors, that rapid cooling was underway by 17 Ma. (c) Enlargement of the plot for the White Hills samples with an AFT age <24 Ma. It is clear from this plot, taking into account errors, that rapid cooling was underway by 17 Ma, perhaps even by 18 Ma. Note the two squares defined by dashed lines: these include two open triangles for samples that were collected from the upper plate and hence are not considered when determining the onset of rapid cooling of the lower plate and also sample WH00-7 (Climax Mine, AFT age of 19.5 ± 2.9 Ma) that, because of its large error, is not considered to reliably indicate an earlier onset rapid cooling than 17–18 Ma.

curve where the variation of age with paleodepth is significant [*Fitzgerald*, 1992]. It is unlikely that offset in the age-paleodepth profile would be revealed in samples below the base of exhumed PAZ/PRZs because the variation of ages with paleodepth is not significant. For example, in the northern part of the crystalline Gold Butte block, *Brady et al.* [2000] showed three low-angle normal faults (Figure 4). Because these faults crosscut the region where AFT ages are rapidly cooled (Figure 3c), any offset along these faults is unlikely to be revealed by an offset of AFT ages unless normal slip exceeded 2.5 km (for the most eastern fault) thereby downdropping higher crustal levels (with older AFT ages, i.e., those from the exhumed PAZ) to the sample location VM89-05. This is not the case. Because the thermochronology results have overlapping exhumed PAZs (apatite and zircon) and PRZs (titanite and zircon) (Figures 3c and 5a) from the nonconformity at the base of the Tapeats Sandstone to ~8.5 km below the nonconformity, it is likely that the Gold Butte block is a more or less coherent block, at least to a paleodepth of ~8.5 km below the sub-Cambrian nonconformity.

[34] The new AFT data collected across strike in the southern part of the Gold Butte block (Figure 4) suggest that the age and position of the base of the exhumed PAZ (with respect to paleodepth) does not vary significantly within the Gold Butte block. However, there is an apparent trend of AFT ages becoming older to the south beneath the sub-Cambrian nonconformity. In the northern part of the Gold Butte block, ~100 m below the nonconformity, the oldest AFT age is 50 ± 3 Ma (VM89-01). To the south, ~200 m below the nonconformity, sample PF91-02 has an AFT age of 66 ± 4 Ma (Figure 4). In the southern part of the Gold Butte block the generally westward younging pattern of ages is complicated by the steep topography on the eastern side of the block and east striking faults that offset the overlying Paleozoic sedimentary section and likely extend (at least for some distance) into the basement. This results in some minor disruption in the AFT-paleodepth relationship

as shown in Figure 5a. If there were no offset of AFT ages (i.e., no faulting), all the samples would lie on the same age-paleodepth line. In fact most samples, within error, do lie on the same line, the obvious exception being sample VM01-10 with a poorly constrained AFT age of 58 ± 11 Ma (1σ). This sample, collected in a region of steep topography, lies off the age-paleodepth trend (i.e., this sample is "too old" and should be much younger given its apparent paleodepth) and thus it is likely that faults, or extensions of faults such as the low-angle Million Hills Wash fault (Figure 4), disrupt the upper portions of the Gold Butte block. In this case, sample VM01-10 would lie on the downdropped side of a normal fault. Whereas such faults are relatively easy to recognize and map in the Paleozoic strata [*Brady et al.*, 2000], they are very difficult to see in the underlying crystalline basement. Interestingly, the easternmost sample of *Reiners et al.* [2000], south of VM01-10 but on the east side of a projected Million Hills Wash fault, had a titanite (U-Th)/He age and an AFT age (unpublished data mentioned by *Reiners et al.* [2000]) that were "too young" with respect to its structural position. *Reiners et al.*'s [2000] interpretation was similar to our conclusion, but their sample lay on the upthrown side of this low-angle normal fault.

[35] *Fitzgerald et al.* [1991] collected one sample (VM89-09, a retrograded garnet gneiss very close to the chlorite breccia zone of the Lakeside Mine fault) from the deepest crustal levels (western portion of the Gold Butte block), that yielded an "old" age of 77 ± 3 Ma (1σ). This result was not consistent with its position near the base of a tilted crustal section. They explained the old age as a fragment of gneiss excised from the hanging wall from a higher crustal level, farther to the south–southeast than their structurally highest samples. We recollected a sample (VM90-03) from the same outcrop and although the apatites were of extremely poor quality, it yielded an age of 20 ± 4 Ma (1σ), based on only 7 grains. There was no doubt that sample VM89-09 had an AFT age of ~77 Ma, but given this new age on VM90-03 and the many new AFT ages from just beneath the sub-Cambrian nonconformity (Figure 4), it is unlikely that large-magnitude excisement of basement from a higher structural level took place. However, this does not preclude finer-scale excisement. Aside from being some of the deepest crustal level samples collected, samples VM89-09 and VM90-03 are also the most southerly samples collected in the Gold Butte block. There are no AFT ages from samples close to the nonconformity that are directly up section of samples VM89-09 and VM90-03, but if there were, we would expect them to give older AFT ages because of the apparent north-to-south trend of older ages under the nonconformity. Four samples collected up section of sample site VM89-09 to address this question all failed to yield sufficient quality apatite. Therefore, the original explanation by *Fitzgerald et al.* [1991] for the 77 Ma AFT age, that a small piece of basement with an AFT age of ~77 Ma from directly beneath the nonconformity was incorporated into the fault zone, remains a possibility. Overall, the thermochronology data from *Fitzgerald et al.* [1991], *Reiners et al.* [2000], and the new data presented herein support that the Gold Butte block is a tilted crustal block exhumed by the low-angle, top-to-the-west Lakeside Mine fault.

6.3. Paleogeothermal Gradient

[36] There are a number of ways to constrain the pre-extensional paleogeothermal gradient based on the available data as follows:

[37] 1. Use the paleodepth of the base of the exhumed apatite PAZ below the sub-Cambrian nonconformity adding the estimated thickness of Paleozoic strata. *Brady et al.* [2000] determined the stratigraphic thickness of the preextensional (i.e., dominantly the Paleozoic strata, plus the Miocene Horse Spring Formation that has a concordant dip with the underlying Paleozoic strata) as 3.5–4 km. If we use a thickness of 3.5 km for the sedimentary strata plus the thickness of crystalline basement between the sub-Cambrian nonconformity and the paleodepth of the base of the exhumed PAZ (~1.6 km) representing the paleo-110°C isotherm, and a paleomean annual temperature of ~10°C, we can constrain the preextensional (early Miocene) paleogeothermal gradient as 110°C–10°C/5.1 km = ~20°C/km.

[38] 2. Use the paleodepth of the base of the exhumed zircon and titanite (U-Th)/He PRZs (~200°C [*Reiners et al.*, 2000]), then using the same approach as above, the preextensional (early Miocene) paleogeothermal gradient can be constrained as 200°C–10°C/10 km = ~19°C/km.

[39] 3. Use the paleodepth of the base of the exhumed zircon PAZ (~240°C [*Bernet*, 2002]); then using the same approach as above the preextensional (middle Miocene) paleogeothermal gradient can be constrained as 240°C–10°C/12 km = ~19°C/km.

[40] 4. Using the difference between the base of the exhumed apatite PAZ (~110°) and the base of the exhumed zircon and titanite (U-Th)/He PRZs (~200°C) divided by the crustal thickness between them yields an estimate of 200°C–110°C/4.9 km = ~18°C/km.

[41] 5. Using the difference between the base of the exhumed apatite PAZ (~110°C) and the zircon PAZ (~240°C) divided by the crustal thickness between them yields an estimate of 240°C–110°C/6.9 km = 19°C/km.

[42] 6. Using the difference between the base of the exhumed zircon and titanite (U-Th)/He PRZs (~200°C) and the zircon PAZ (~240°C) divided by the crustal thickness between them yields an estimate of 240°C–200°C/2 km = 20°C/km. Using these approaches, the paleogeothermal gradient just prior to late early Miocene extension is constrained as 18–20°C/km.

6.4. Slip Rate

[43] As discussed above, the slip rate along a low-angle normal fault can be constrained if samples are collected parallel to the extension direction and if the fault approximately parallels the land surface. The Lakeside Mine segment of the SVWHD [*Wernicke and Axen*, 1988; *Duebendorfer et al.*, 1998; *Brady et al.*, 2000] is mapped as nearly parallel to the land surface (Figure 3b). A weighted regression line, incorporating errors in AFT age and location, plotting AFT age for rapidly cooled samples versus

distance from the sub-Cambrian nonconformity yields a (minimum) slip rate of 8.6 ± 6 km/Ma (1σ) along the Lakeside Mine fault during tectonic exhumation and tilting of the Gold Butte block (Figure 5b). If there was systematic incisement (transfer of lower plate rocks to the upper plate during exhumation [*Lister and Davis*, 1989]), the variation of age with horizontal distance would not represent the slip rate. In the Whipple metamorphic core complex, *Stockli et al.* [2006] suggested that crustal incisement has lead to crustal duplication, and therefore a slip rate determined from plotting all data (~4–6 km/Ma) is actually an overestimate, and that if different detachment faults are operating at different times, the rate of slip on each is actually much less (1–2 km/Ma). In the case of the Gold Butte block, while there are some low-angle normal faults within the block (Figure 4), their importance appears to be minor as they do not significantly offset the overlapping exhumed AFT PAZ, the exhumed titanite and zircon (U-Th)/He PRZs and the exhumed zircon FT PAZ (Figure 3c). Thus, significant crustal incisement is not apparent and slip rate on the Lakeside Mine fault is likely to be on the order of 8.6 km/Ma.

6.5. Original Dip of the Lakeside Mine Fault

[44] In the restored cross section of *Wernicke and Axen* [1988], the original dip of the Lakeside Mine fault is ~60°. *Brady et al.* [2000], in a more extensive evaluation of the kinematic evolution of the Gold Butte block, likewise concluded that extension was accommodated initially on moderately to steeply dipping listric normal faults, although some early faults were active at dips <20°. Isostatic uplift and domino-style rotation of fault blocks later rotated the original steeply dipping faults to subhorizontal such as portrayed in Figure 3b.

[45] Low-temperature thermochronology has been used as one of the methods in constraining the original dips of detachment faults in many extended regions, including the Basin and Range province. There are several approaches for constraining initial fault dips using thermochronology (as summarized by *Stockli* [2005]). We used constraints for the horizontal position of the base of the AFT PAZ, the base of the zircon and titanite PRZs and the well constrained (see above) preextensional geothermal gradient of 18–20°C/km to determine an initial dip of ~35° for the Lakeside Mine fault (Figure 7a). Taking into account uncertainties on the location of the PAZs and the PRZs within the Gold Butte block (±200 m) and also the temperatures for these (±5°C for the PAZ and ±10° for the PRZs), yields an initial dip of 28–43°. This dip is somewhat less than that proposed by *Wernicke and Axen* [1988], and could be construed at first glance to suggest that the Lakeside Mine fault was initiated as a low-angle fault and accommodated slip at a gentle dip. However, possible additional postextensional tilting of the Gold Butte block as discussed above [*Howard et al.*, 2000], brings our estimate of the initial dip closer to that proposed by *Wernicke and Axen* [1988]. Because of the uncertainties in constraining paleodips of faults (see assumptions as listed on Figure 7a and discussed by *Foster and John* [1999] and *Stockli* [2005]) the estimates for fault dips derived herein are not robust enough to overturn the view of Gold Butte as a tilted crustal block with an initial fault dip of ~60°. However, our estimates do suggest that the initial dip on the major controlling structure for the tectonic exhumation of the Gold Butte block was more moderate than steep. Note that extrapolation of the best fit line to the base of the Tapeats Sandstone provides an independent measure of the thickness of the Paleozoic section prior to cooling due to tectonic exhumation at ~3.7 km, in good agreement with *Brady et al.* [2000].

6.6. A New "Vector" Approach to Constraining Fault Dip During Slip Using Low-Temperature Thermochronology

[46] We also apply a new approach, derived using this data set, for constraining the dips on faults. This approach (Figure 7b) relies on the fact that the Gold Butte block is a largely intact tilted crustal block and we can plot sample location versus paleodepth (Figure 5a) and also plot sample location versus horizontal distance on a line parallel to the extension direction (Figure 5b). The slope of a weighted regression line fit to AFT age versus paleodepth for rapidly cooled samples yields a vertical exhumation rate of 7.2 ± 4.9 km/Ma ($\pm1\sigma$). As discussed above, this slope will be a minimal estimate on the vertical exhumation rate. The slope of a weighted regression line fit to AFT age versus horizontal distance yields a slip velocity of 8.6 ± 6.0 km/Ma ($\pm1\sigma$). The vertical exhumation rate and the slip rate are vectors, thus the angle between them ($\phi \sim 33°$) can be used to constrain the dip of fault ($90 - \phi$) as ~57° during movement of the fault (Figure 7b). This value is more in line with the original estimates of the fault dip of *Wernicke and Axen* [1988]. However, the large uncertainties on the vertical exhumation rate and the slip rate means that the fault dip using this approach is poorly constrained. Despite the large uncertainties, we include this new approach in this paper as with more samples and better precision [e.g., *Carter et al.*, 2004, 2006], it may provide valuable constraints in other extensional terranes.

[47] Caveats to this vector approach include constraining the paleodepth, either an absolute preextension value (as is done herein) or simply the "variation of the samples with apparent paleodepth" in order to constrain a vertical exhumation rate. In situations like the Gold Butte block, where dip of sedimentary strata allow restoration of the block to its preextension orientation and samples to their preextension (preslip) depth, this exercise is relatively straightforward if a planar fault is assumed [*Reiners*, 2005]. However, if the active exhuming fault was listric, then the real depth of each sample will be shallower than estimated assuming a planar fault, and so the paleodepth will be an overestimate, with the discrepancy increasing with sample depth. Hence the vertical exhumation rate will also be an overestimate, ϕ will be smaller than it should be, and the constrained dip will therefore be steeper, i.e., an overestimate of the actual dip of the exhuming fault. Another caveat is the evolving dynamic thermal state of the crust [*Ehlers*, 2005] during extension and correcting for the advection and perturbation of the isotherms when calculating the vertical exhumation rate and

the slip rate, both of which will be minimal values). Advection in such a rapidly extending region will cause a preextension geothermal gradient (e.g., 20°C/km) to rapidly transition into a higher geothermal gradient (e.g., 50°C/km).

[48] Nonetheless, this vector approach potentially provides a mechanism to constrain the evolution of the dip of the fault throughout its history (Figure 7c) through application to different thermochronometric systems, each with a different closure temperature. Thus a higher temperature method would constrain the dip of the exhuming fault at a higher temperature (deeper crustal level, earlier part of the history) and a lower temperature method at a lower temperature (shallower crustal level, later part of the history). For example, in the rolling hinge model, a steeper fault dip would be predicted for higher temperature methods as compared to lower temperature methods. However, given the uncertainties on vector magnitudes we cannot differentiate between the slopes of the various chronometers for

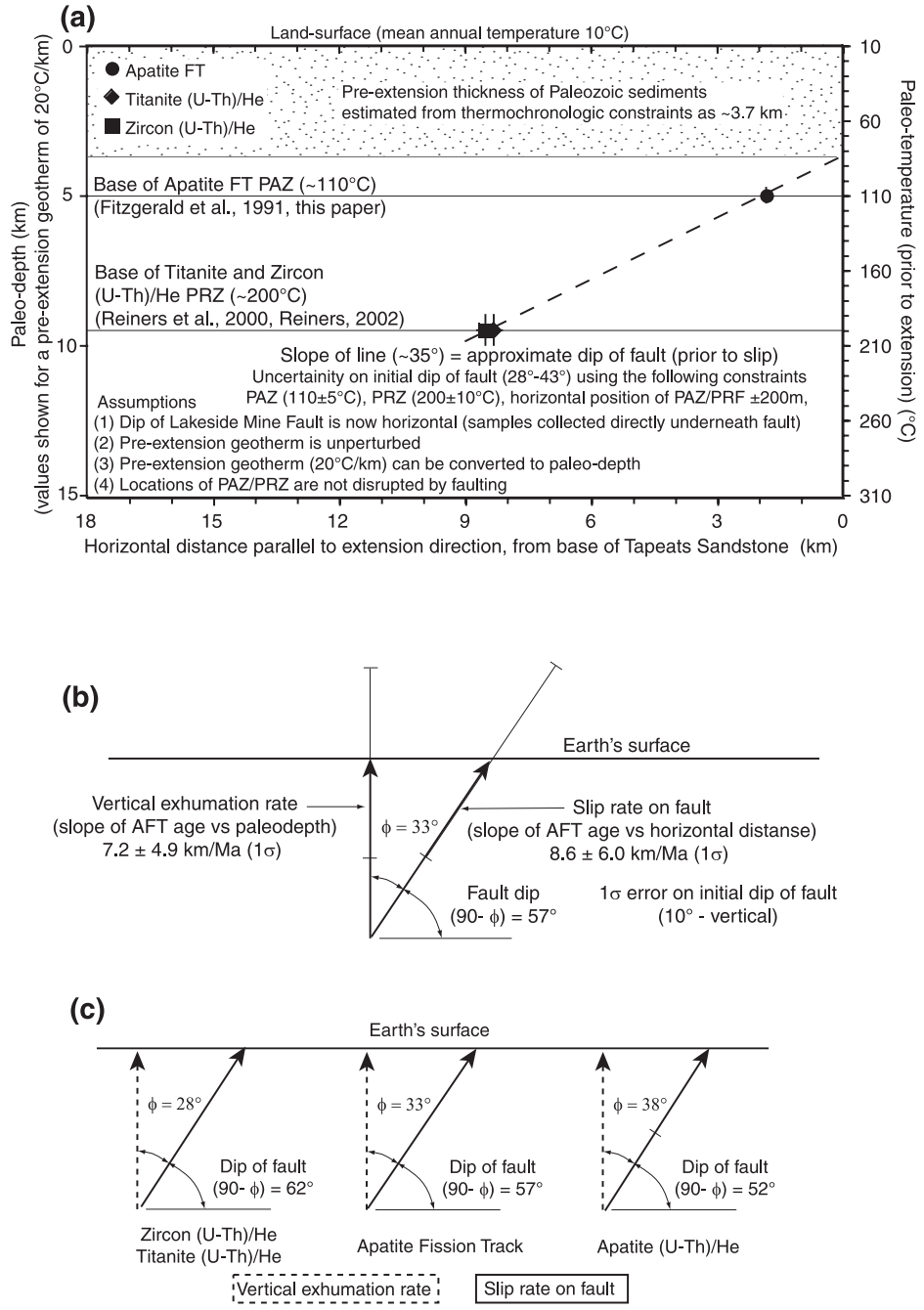

Figure 7

paleodepth versus age to anywhere near the precision required, and hence we cannot determine fault dip evolution at this time.

[49] Different thermochronometers also have different response times to cooling. In other words, higher temperature methods are slower to respond to a cooling surface [*Ketcham*, 1996; *Reiners and Brandon*, 2006]. However, if the rate of cooling is sufficiently rapid, the differential response time among thermochronometers is minimal, certainly not the greatest uncertainty in this approach. In essence this means that with thermochronometers of differing closure temperature, taking into account the higher closure temperatures due to rapid cooling, we are potentially sampling the evolution of fault dip over a temperature interval of ~70°C to ~270°, a 200°C crustal equivalence of ~4 km. Given the magnitudes of vertical exhumation rate and slip rate on these extensional terranes (order of km/Ma), the age difference between methods may be minimal and require high-precision ages, many samples, and suitable lithologies to constrain fault dip evolution. Nevertheless, despite being in its infancy, this new vector approach does offer another method for constraining fault dip and possibly fault dip evolution during slip.

6.7. Gold Butte Block Summary

[50] The evidence that the Gold Butte block is a ~15 km thick easterly tilted crustal block, exhumed by westward dipping normal faults is based on structural, petrologic and geobarometric evidence [*Wernicke and Axen*, 1988; *Fryxell et al.*, 1992]. The first systematic low-temperature thermochronology study of the Gold Butte block [*Fitzgerald et al.*, 1991] was consistent with the Gold Butte block as an easterly tilted crustal block with the onset of rapid cooling due to tectonic exhumation as a result of extension, initiated at ~15 Ma. *Reiners et al.* [2000] concluded the onset of rapid cooling was at 15–16 Ma. With our new data, we suggest the initiation of rapid cooling was slightly earlier, ~17 Ma.

[51] On the basis of mapping of the Tertiary Horse Spring Formation northwest and southeast of the Gold Butte block, *Beard* [1996] concluded that the entire Paleozoic section was most likely eroded from part of the Gold Butte block prior to extension and that large areas of the crystalline basement were at shallow levels prior to Miocene extension. The ~77 Ma AFT age from the western part of the Gold Butte block obtained by *Fitzgerald et al.* [1991] was cited by *Beard* [1996] as supporting evidence that this part of the block was at shallow levels, rather than being an excised portion of the upper plate, although the AFT age-paleodepth relationship was not addressed by *Beard* [1996]. The study by *Beard* [1996] implied that the Gold Butte block is not a largely intact crustal block exhumed and tilted along west dipping normal faults. However, the age-paleodepth relationship (Figure 3c) of multiple low-medium temperature thermochronometers is unequivocal, indicating a continuous depth-temperature increase and that these samples were not all at shallow levels prior to Miocene extension [*Fitzgerald et al.*, 1991; *Reiners et al.*, 2000].

[52] Thus the Gold Butte block is most simply interpreted as a largely intact tilted crustal block as suggested by *Wernicke and Axen* [1988] and in subsequent papers by *Fryxell et al.* [1992] and *Brady et al.* [2000]. Prior to extension the paleogeothermal gradient can be constrained as 18–20°C/km, and ~3.7 km of Paleozoic and younger strata rested on the Proterozoic basement. While the initial dip of the fault cannot be better constrained using two thermochronologic methods, the results are consistent with structural reconstructions that indicate a steep to moderate (~60°) initial dip and subsequent rotation to a gentle dip. The slip rate on the fault was ~8.6 km/Ma.

7. White Hills–Lost Basin Range–Colorado Plateau: Results and Discussion

7.1. Structural Setting

[53] The overall structure of the White Hills region is not as straightforward as the Gold Butte block because the White Hills region is not a single largely intact crustal block tilted to the east. Rather, a series of major north striking

Figure 7. Methods used to determine the initial dip of the Lakeside Mine fault. (a) Plot of the position of the exhumed base of the apatite PAZ (110 ± 5°C) and the exhumed base of the zircon and titanite PRZs (200 ± 10°C) versus horizontal distance on a line measured parallel to the extension direction. Sample position is projected onto this line. The location of the base of the PAZ/PRZ is best identified on a paleodepth versus distance plot (Figures 3c and 5a). The depth to the position of the base of the PAZ/PRZ is determined using the constrained preextensional geothermal gradient (18–20°C/km) as discussed in the text. The initial angle of the fault is simply the dip of the best fit line between the positions of the PAZ and PRZ. The constraints that are required to make this determination are listed on the figure but include that the fault dip is currently near horizontal (i.e., samples collected on the land surface are near equidepth below the fault) and that samples are collected beneath the fault and that sample position (to determine the depth/location of the base of the PAZ/PRZs) is not disrupted by faulting. (b) New "vector" approach to determine the dip of major faults [*Fitzgerald*, 2006]. The slope of AFT ages versus paleodepth is equal to the vertical exhumation rate. The reciprocal slope of the AFT age versus horizontal distance for rapidly cooled samples projected onto a line parallel to the extension direction is equal to the slip rate along the fault. Treating the vertical exhumation rate and the slip rate as vectors, the angle (ϕ) between them constrains the dip of the fault ($90 - \phi$ = fault dip). Using this approach, the dip of the Lakeside Mine fault as it slipped was ~57°, although as can be seen from the diagram, the errors on the regression lines for the vertical exhumation rate and the slip rate along the fault make for a large uncertainty on the dip of the fault. (c) Hypothetical example of this vector approach for a rolling hinge model in which the dip of the fault starts at a steeper angle and then shallows.

faults divide the region into two distinct ranges between the SVWHD and the relatively undeformed Grand Canyon region of the Colorado Plateau, where Proterozoic basement is capped by gently dipping or flat-lying Paleozoic strata (Figure 2). The Grand Wash fault marks the dramatic and scenic edge of the Colorado Plateau. This fault (or fault zone [*Lucchitta*, 1966; *Lucchitta and Young*, 1986; *Faulds et al.*, 1997; *Brady et al.*, 2000; *Faulds et al.*, 2001b]) separates the Gold Butte block, the Wheeler Ridge block, and the Lost Basin Range from the Colorado Plateau. Offset on this steeply dipping listric normal fault (or faults) is estimated at 3.5–5 km [*Matthews*, 1976; *Faulds et al.*, 1997; *Brady et al.*, 2000; *Faulds et al.*, 2001b] with movement from ~16 to 11 Ma [*Faulds et al.*, 2001b]. As discussed above, however, the dominant structure in this region is the west dipping, low-angle, top-to-the-west SVWHD, expressed in the White Hills as the Salt Spring and Cyclopic Mine faults.

[54] On the west flank of the Lost Basin Range lies the Lost Basin Range fault, and its likely northeast en echelon extension, the Wheeler Ridge fault [*Wallace*, 1999; *Blythe*, 2005; *Swaney*, 2005; *Wallace et al.*, 2005]. The Lost Basin Range fault is a down-to-the-west listric normal fault with at least 500 m of displacement as indicated by the topographic relief on the west side of the Lost Basin Range. Movement on this fault must have continued until after 6 Ma, as the 11–6 Ma strata of the Hualapai Limestone on the southeast end of the Lost Basin Range are tilted and cut by the fault [*Lucchitta*, 1966; *Wallace*, 1999; *Howard et al.*, 2000; *Wallace et al.*, 2005]. The Wheeler Ridge fault was mapped by *Longwell* [1936] as a steeply dipping, down-to-the-west normal fault with ~2.1 km of offset where it crosses Lake Mead [*Brady et al.*, 2000]. Near the south end of Wheeler Ridge this fault splits into several splays and essentially terminates as strain transfers westward to the Lost Basin Range fault in a broad north facing relay ramp [*Wallace*, 1999; *Blythe*, 2005; *Swaney*, 2005; *Wallace et al.*, 2005].

[55] The Meadview fault is a normal fault, down to the northeast, separating Proterozoic basement and nonconformably overlying Paleozoic strata of south Wheeler Ridge from Proterozoic basement of the northern Lost Basin Range. A 100 m wide damage zone implies that this fault has accommodated significant displacement [*Swaney*, 2005].

7.2. Apatite Fission Track Age Patterns

[56] Reflecting the more complex structural setting in the White Hills, the distribution of AFT ages is not as straightforward as in the Gold Butte block. Basically, AFT ages in the White Hills can be separated into two main groups (Figure 8). West of the Meadview fault in the footwall of the SVWHD, AFT ages are all <20 Ma and in general the track length distributions reflect rapid cooling. East of the Meadview and Grand Wash faults AFT ages are all >60 Ma and track length distributions reflect a more complex thermal history with samples residing for considerable time in the apatite PAZ. AFT results are discussed in the context of these two groups. In the White Hills within the footwall of the SVWHD, there is no single (semicoherent) tilted crustal block with an overlying unconformable sedimentary section. Thus, it is not possible to plot these samples according to paleodepth.

[57] The most profound break in AFT ages is across the Meadview fault, where on the southwest side there are rapidly cooled samples (determined from track length data) with AFT ages of 15.3 ± 1.2 Ma and ~18–19 Ma. In contrast, only ~2 km away on the northeast side of this fault, there is an AFT age of 127 ± 8 Ma with a shorter mean length indicative of a more complex thermal history. This profound age difference implies that: (1) Any original exhumed PAZ east of the SVWHD in the White Hills region (compare to the Gold Butte block), has likely been uplifted and eroded owing to movement along the Meadview Fault and the SVWHD. (2) The Meadview fault is one of the more important structures in this region and likely continues south along the east flank of the Lost Basin Range to at least the Garnet Mountain area. However, the Meadview fault is almost entirely covered by late synextensional to postextensional sedimentary rocks of the Grand Wash trough bracketed between ~15.3 Ma and 13 Ma by $^{40}Ar/^{39}Ar$ ages on tuffs near the base of and within the section [*Faulds et al.*, 2001b; *Blythe*, 2005; *Wallace et al.*, 2005]. This indicates that movement on the Meadview fault had ceased sometime between ~15.3 and 13 Ma, possibly during or immediately after the major pulse of extension on the SVWHD, from ~16 to 14 Ma [e.g., *Beard*, 1996; *Duebendorfer and Sharp*, 1998; *Price and Faulds*, 1999; *Faulds et al.*, 2001b, 2009; *Blythe*, 2005].

[58] The east dipping Meadview fault may have served as a major antithetic fault that accommodated uplift of the footwall of the SVWHD (Figures 8 and 9). Thus, it would have been active contemporaneously with the SVWHD and most active during peak extension (~16.5 to 15 Ma), thereby helping to accommodate footwall isostatic uplift induced by large-magnitude extension along the SVWHD. Once extension waned, however, it no longer served an important kinematic role, so it became inactive by ~13 Ma. Accommodation of footwall uplift may have been favored in the vicinity of the Lost Basin Range, as opposed to within the more stable block of the Colorado Plateau directly to the east.

[59] Another significant break in AFT ages is between the southern Lost Basin Range and the northwesternmost point on Garnet Mountain where the AFT age jumps from 15 Ma to 68 Ma in a ~5 km distance. There is a similar jump in ages across the alluviated valley between the southern White Hills and the Cerbat Mountains. AFT ages in the southern White Hills are ~16 Ma while to the south in the Cerbat Mountains there is a 73 Ma age. We interpret these data to indicate that: (1) The marked contrast in AFT dates between the southern Lost Basin Range and Garnet Mountain may correspond with the buried trace of a southern extension of the Meadview fault. (2) The Meadview fault is significant, much more so than initially considered. (3) The contrast in AFT ages between the southern White Hills and the Cerbat Mountains may result from the northward

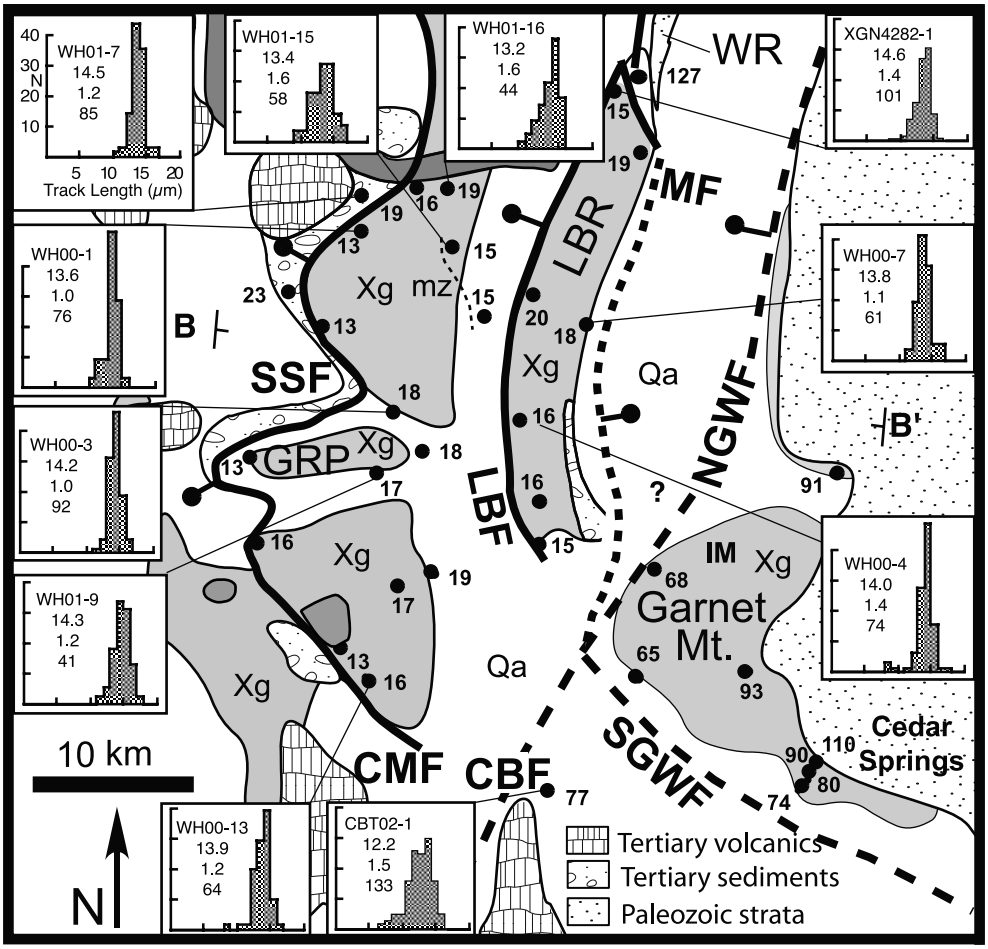

Figure 8. (top) Geological sketch map of the White Hills region with representative AFT confined track length distributions (e.g., WH01-7 has a mean length of 14.5 μm and a standard deviation of 1.2 μm, and 85 tracks were measured). Abbreviations are as for Figures 1 and 2. (bottom) Diagram of west–east cross section (B-B′) through the White Hills region from Salt Spring fault to the Colorado Plateau (modified after *Kelleher* [2001]). Note that this cross section implies that the Lost Basin Range is an eroded tilt block in the hanging wall of the Grand Wash fault(s) [*Brady et al.*, 2000], although this appears unfeasible based on the amount of erosion required off the top of the Lost Basin Range following faulting, in order to expose 18–20 Ma AFT ages (see text for discussion).

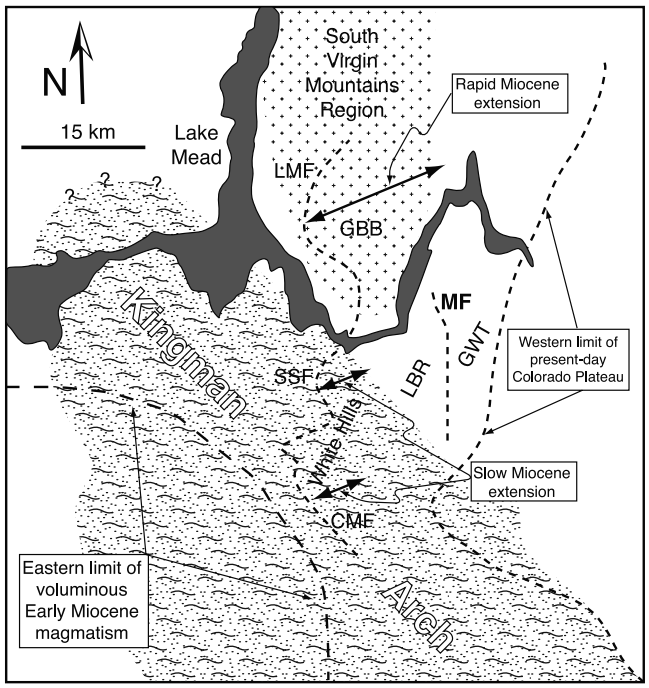

Figure 9. Simplified paleogeographic sketch map of part of southwestern Nevada and northwest Arizona prior to Miocene extension. Abbreviations are as for Figures 1 and 2, including GBB, Gold Butte block. The present-day location of the SVWHD (parts are labeled as LMF, SSF, and CMF), Meadview fault (MF) are also shown. Inferred location of the Kingman Arch is from *Beard* [1996] that is based on the work by *Lucchitta* [1966] and *Bohannon* [1984]. The eastern limit of voluminous early Miocene magmatism is from *Faulds et al.* [1995, 1999, 2001a, 2009].

increase in offset along the SVWHD and concomitant northward increase in tectonic denudation.

7.3. West of the Grand Wash Fault (White Hills and Lost Basin Range)

[60] AFT ages west of the Meadview and Grand Wash faults and east of the SVWHD (i.e., in the lower plate of the SVWHD) range from 12.6 ± 1.8 Ma to 19.8 ± 2.9 Ma. Mean track lengths range from 13.2 μm to >14.5 μm and standard deviations are all $\leq$1.6 μm. We interpret these data to reflect rapid cooling (with modification to some samples) due to tectonic exhumation associated with extension in this region controlled by the SVWHD. In general we would expect all AFT ages and track lengths from the lower plate of a major low-angle detachment to reflect rapid cooling, and therefore have mean lengths >$\sim$14 μm, but in this area a few samples have mean lengths and distributions indicative of later annealing. The majority of such samples (WH00-1, WH00-6, WH01-15, WH01-16), with mean lengths <13.8 μm, come from lower plate exposures near Lake Mead. Thermal effects induced by hydrothermal activity associated with Miocene magmatism may account for the partial annealing of these samples, resulting in slightly reduced mean lengths. It is noteworthy that hydrothermally altered basement rocks and Miocene basalts (K/Ar date of 10.9 ± 0.6 Ma [*Theodore et al.*, 1987]) are present in this area (Figures 1 and 2).

7.3.1. Timing of Extension

[61] In the lower plate of the SVWHD we do not see a clear-cut transition to rapidly cooled ages (parallel to the extension direction) from samples that have resided in a PAZ, and there is no exhumed PAZ preserved, as is the case for the Gold Butte block. Thus, the control on the onset of rapid cooling due to tectonic exhumation accompanying extension is less well constrained than at the Gold Butte block. However, as all samples in the lower plate indicate rapid cooling, including those samples that underwent later annealing (as discussed above), the onset of rapid cooling must predate the age of the oldest rapidly cooled sample, $\sim$18 Ma (Figure 6c). There are a couple of samples >18 Ma with track length distributions indicative of rapid cooling (WH00-7, 19.5 ± 2.9 Ma, mean length of 13.8 μm; WH01-14, 19.8 ± 2.9 Ma, mean length of 14.7 μm), but these have large errors and/or only a small number of measured confined lengths. These data essentially agree with previous estimates of an $\sim$16.5 Ma onset of major extension in the region [e.g., *Faulds et al.*, 1995; *Beard*, 1996; *Duebendorfer et al.*, 1998; *Faulds et al.*, 1999; *Price and Faulds*, 1999; *Faulds et al.*, 2001a; *Wallace et al.*, 2005]. These previous estimates were based on tilt fanning within Miocene strata and initiation of major growth fault basins, the timing of which is tightly constrained in several cases by high-precision $^{40}Ar/^{39}Ar$ dating of multiple volcanic units [e.g., *Faulds et al.*, 1995].

[62] Two samples were collected from the upper plate in Salt Spring Wash, proximal to the Salt Spring fault. WH01-6 is rhyolite lithic tuff dated by $^{40}Ar/^{39}Ar$ sanidine at 15.2 Ma [*Duebendorfer and Sharp*, 1998]. The AFT age of 23.0 ± 1.5 Ma is clearly older than the age of the tuff; therefore this sample must include xenocrystic material. WH01-7 is a megacrystic granite clast from a megabreccia within the upper plate. Its age of 18.9 ± 1.7 Ma and mean length of 14.5 μm clearly indicate it was eroded from exposed crust of the lower plate that had already been exhumed to the surface by $\sim$18 Ma. This result is consistent with the interpretation that rapid cooling of the lower plate was underway by $\sim$18 Ma.

[63] Rapid cooling due to tectonic exhumation accompanying extension was therefore underway at approximately the same time in the White Hills as the Gold Butte block. This result negates hypothesis 2, that exhumation of the SVWHD along-strike was diachronous.

[64] The youngest ages in the lower plate of the SVWHD in the White Hills are $\sim$13 Ma (WH00-2, 12.6 ± 1.8 Ma; WH01-8, 13.3 ± 1.8 Ma; WH02-2, 12.8 ± 3 Ma), indicating that rapid cooling and hence tectonic exhumation continued until at least then. These data are compatible with tilt relations in the area [*Beard*, 1996; *Duebendorfer and Sharp*, 1998; *Price and Faulds*, 1999; *Faulds et al.*, 2001b;

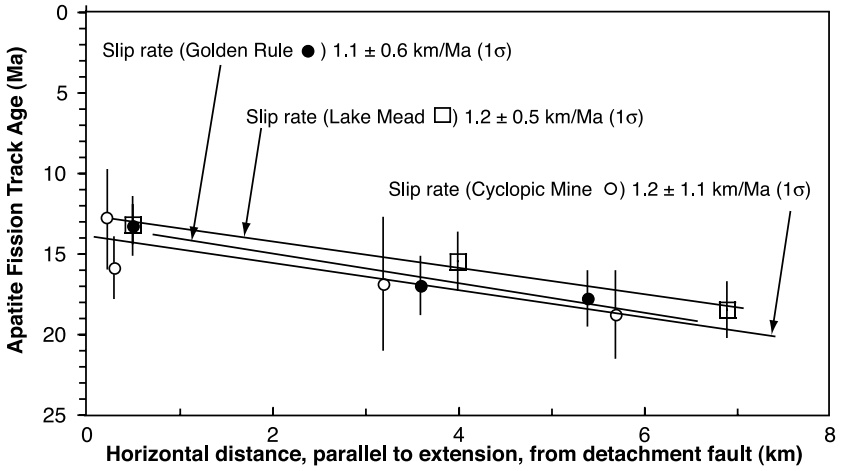

Figure 10. AFT age for rapidly cooled samples plotted against horizontal distance (parallel to extension direction) from the detachment fault. The slope of the line for rapidly cooled samples is proportional to the slip rate on the fault. The Lake Mead transect is in the northern part of the White Hills, Golden Rule Peak in the central part of the White Hills, and Cyclopic Mine in the south part of the White Hills. Note the similarity in slip rate, especially compared to the much more rapid slip rate in the Gold Butte block.

Wallace et al., 2005] that indicate a major phase of extension between ~16.5 and 13 Ma, although minor extension continued to at least ~8 Ma in the southern White Hills and post 6 Ma in the Lake Mead area.

7.3.2. Slip Rate

[65] We apply the same approach to constrain slip rate in the lower plate of the Salt Spring fault and the Cyclopic Mine fault as we did in the Gold Butte block. In such a scenario there should be an overall progression of ages becoming older from west to east, parallel to the extension direction. Such a pattern of AFT ages does occur in the lower plate of the Salt Spring and Cyclopic Mine faults as would be expected because of progressive exhumation of the footwall in the direction of upper plate translation. However, this pattern is complicated by four elements:

[66] 1. AFT ages have relatively large errors because of the statistics associated with the number of fission tracks counted, but the precision of the technique is often exacerbated in poor quality samples such as those collected from fault rocks and in zones of alteration in old mines (e.g., WH00-7, Climax Mine; WH01-14, Golden Gate Mine).

[67] 2. Samples close to Lake Mead may have experienced a partial thermal overprint, likely by Miocene hydrothermal activity as discussed above, and as evidenced by slightly reduced mean lengths.

[68] 3. *Coven* [2005] mapped a 40° west dipping chlorite phyllonite zone in the Hualapai Valley directly west of the Lost Basin Range fault. Two samples collected 10–50 m structurally below this phyllonite zone gave AFT ages of ~15 Ma. These samples are younger than samples to the west. Although this fault zone is not as significant as the Salt Spring fault to the west, this apparent offset in the expected age trend suggests that this fault zone was active synchronously with the SVWHD.

[69] 4. Although apparently not as significant as *Coven*'s [2005] phyllonite zone, the more topographically obvious Lost Basin Range fault, with its down-to-the-west normal offset of ≥500 m, appears to also interrupt the age progression.

[70] Because of these complications to the structural integrity of the lower plates of the Salt Spring and Cyclopic Mine faults and because of the danger of incisement and crustal duplication, as discussed above, we limit the selection of samples to constrain the slip rate to those west of the newly mapped fault zone of *Coven* [2005] and west of the Lost Basin Range fault. As discussed in section 7.2, the role of the Meadview fault in the exhumation of the White Hills is not well constrained, but all samples used in the determination of the slip rate are relatively proximal to the Salt Spring and Cyclopic Mine faults and well west of the Meadview fault, and all age trends indicate exhumation of these samples was via slip on the SVWHD.

[71] We determine slip rate on three limited transects: (1) near Lake Mead, (2) near Golden Rule Peak, and (3) near Cyclopic Mine. Note that all three of the samples near Lake Mead were slightly annealed, presumably by Miocene hydrothermal activity, but for the purpose of estimating slip rate, we assume that these samples are annealed a similar amount. Also, because of the limited extent of footwall between the detachment fault and the Lost Basin Range fault, there are only 3–4 points per transect. However, the determined slip rates are remarkably similar (Figure 10) at 1.1–1.2 km/Ma. These slip rates are dramatically less than that determined for the Lakeside Mine fault at Gold Butte. This result supports the conclusions in section 7.3.1, i.e., that hypothesis 2 (diachronous cooling along the SVWHD) is incorrect and that the displacement gradient along the SVWHD can be explained by hypothesis 1, synchronous

along-strike exhumation with differential slip rates. This result favors growth of the SVWHD by linkage of individual segments as discussed in section 5.

7.3.3. Original Dip of the Salt Spring and Cyclopic Mine Fault

[72] AFT thermochronology allows a very crude semi-quantitative constraint on the original dip of the different segments of the SVWHD in the White Hills region. Using a temperature of 110°C for the base of the AFT PAZ and assuming a preextension geothermal gradient of 18–20°C/km (well constrained at the Gold Butte block but unconstrained in the White Hills), the base of the PAZ would have been at a depth of 5.5–6.1 km. Because all samples west of the Meadview fault (and its implied southward extension) have mean track lengths >14 um (i.e., little or no annealing) they must have been at this depth or deeper prior to extension. If the Salt Spring segment had ~9 km of displacement (unknown, but intermediate between the slip on the Lakeside Mine and Cyclopic Mine faults [*Duebendorfer and Sharp*, 1998]), we can use simple trigonometry to constrain the minimum initial dip on this fault to ~38–43°. Dip on the Cyclopic Mine segment (<6 km displacement) would have been much steeper (60–90°). We emphasize that this is a crude constraint because the paleogeotherm just prior to extension is not known for the White Hills, and it may be higher because of its proximity to ~19–13 Ma volcanism in the northern Colorado River extensional corridor west of the White Hills [e.g., *Faulds et al.*, 1999]. For example if we use a paleogeotherm of 25°C/km, then initial dip on the Salt Springs fault was 29° and on the Cyclopic fault was ~47°. These inferences for initial fault dips are loosely consistent with foliation attitudes in the footwall of the Salt Spring fault, which although variable, generally do not exceed 40° (west). Foliation attitudes on Garnet Mountain and in the Lost Basin Range, which have not been tilted appreciably in the Phanerozoic, strike north–south and are statistically subvertical [*Blacet*, 1975]. Although we recognize the dangers of using the orientations of Proterozoic foliations as indicators of Tertiary tilt, it is worth noting that Proterozoic foliations throughout northwestern Arizona in areas of demonstrably little to no Tertiary tilt (e.g., Garnet Mountain, Lower Granite Gorge of Grand Canyon, Cerbat, and Hualapai Mountains) have only limited domains of low-angle foliations [*Duebendorfer et al.*, 2001], and foliation attitudes are dominantly >70°. Therefore, the relatively low dips of foliation in the footwall of the Salt Spring fault are consistent with tilting of the footwall and the fault from originally steeper orientations.

7.4. East of the Meadview and Grand Wash Faults

[73] All AFT ages from basement rocks east of the Meadview fault and the buried trace of the Grand Wash fault are >60 Ma and have track length distributions indicative of a complex thermal history. AFT ages are oldest directly beneath the basement nonconformity with the Tapeats Sandstone (90–110 Ma) and become younger with structural depth, down to ~65 Ma, ~1.2 km under the nonconformity. Overall, these samples have a relatively complex history reflecting residence in an apatite PAZ prior to Laramide cooling, followed by a period of relatively rapid cooling in the Laramide (70–50 Ma), a possible period of heating initiated in the late Eocene–early Oligocene, and then final cooling at about the same time as tectonic exhumation of the lower plate of SVWHD.

[74] Evidence for Laramide cooling comes from the following: (1) AFT age versus depth below the nonconformity for samples from a relatively tightly clustered vertical profile at Cedar Springs and also samples from Garnet Mountain that indicate the onset of more rapid cooling at ~75 Ma (Figure 11). Note that within the track length distributions, short tracks that survived in samples that resided near the base of the pre-Laramide PAZ can be observed in WH00-9 and WH00-8. Track length distributions from under the break in slope in the profile do not indicate "classic" rapid cooling as is commonly observed in such profiles [*Fitzgerald and Gleadow*, 1990], reflecting either slow cooling through the PAZ, rapid cooling but then residence within the PAZ, or later annealing due to partial thermal resetting. (2) Thermal modeling (Figure 12) clearly shows a period of more rapid cooling from ~80 to ~60 Ma, with some samples below the break in slope (WH00-11-12, WH01-3) having well-constrained T-t paths clearly showing this Laramide cooling. (3) A comparison with other AFT data collected from the Colorado Plateau to the east of this region. *Dumitru et al.* [1994] indicated the onset of Laramide cooling there as ~75 Ma, noting that this age corresponds with the beginning of Laramide deformation in block uplifts north and east of the Colorado Plateau [e.g., *Dickinson et al.*, 1988].

[75] Interestingly, the data (qualitative interpretation supported by thermal modeling, Figure 12) suggest a period of reheating likely initiated during the late Eocene–early Oligocene (~35–30 Ma) before cooling started again in the early Miocene. Although the timing of this reheating event is poorly constrained, it does appear quite significant, on the order of 10–20°C (0.5–1 km of sediment equivalent for a geotherm of 20°C/km) to temperatures possibly exceeding 60°C. Note that we see this reheating event in samples east of the Grand Wash fault, but not in the White Hills (where the AFT ages are too young anyway and this event would not be recorded) or in the Gold Butte block. As such, it is most logical to relate this heating event to burial along the western margin of the Colorado Plateau by Eocene sedimentary rocks ("rim gravels") [e.g., *Young*, 1982] derived from the uplifted Kingman arch to the west rather than to distant volcanism, as magmatism did not occur in this region until ~18.5–19.5 Ma. The timing of the later (early Miocene) cooling suggested by the models is consistent with paleocurrent reversal across the rim of the western Colorado Plateau and consistent with apatite (U-Th)/He data from this region [*Flowers et al.*, 2008]. Other samples collected from higher stratigraphic positions from the Water Pocket Monocline on the Colorado Plateau [*Dumitru et al.*, 1994] also suggested some middle and/or late Tertiary heating possibly due to up to 2–3 km of burial [e.g., *Nelson et al.*, 1992]. In contrast, *Foster et al.* [1993] attributed mid-Tertiary heating, recorded in AFT data from the Weaver and Bradshaw Mountains that lie in the transi-

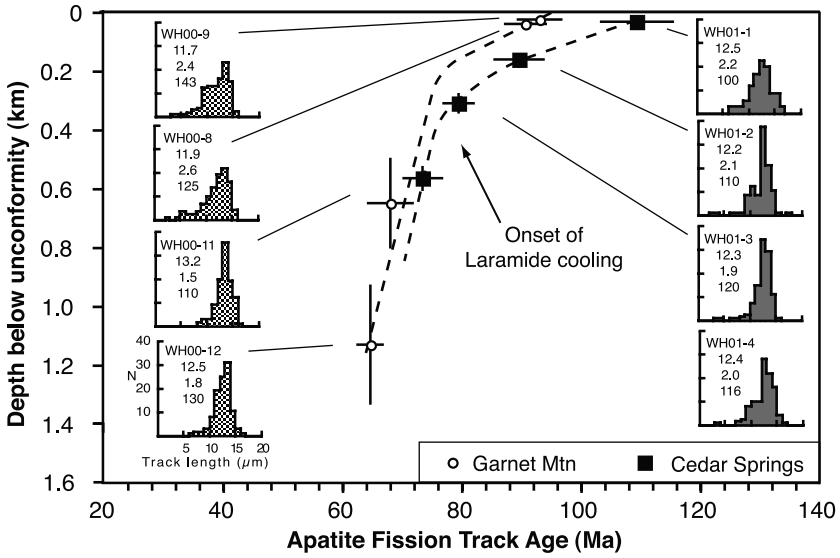

Figure 11. Depth below the Cambrian nonconformity versus AFT age. We plot depth below the nonconformity rather than sample elevation as this more clearly depicts the ''break in slope'' representing the approximate location of the base of an apatite PAZ and hence the onset of cooling associated with the Laramide orogeny. Depth below the nonconformity is calculated using a dip of 168°/7°/E for the Tapeats Sandstone as measured at the top of the Cedar Springs profile. Note that the track length distributions below the break in slope do not depict the classic rapidly cooled distributions that are often present [*Fitzgerald and Gleadow*, 1990] but reflect that the samples did not cool completely through the PAZ and also suggest a later Oligocene–Miocene phase of heating (as seen in the thermal models in Figure 12). Confined track length distributions list the sample number, mean and standard deviation in microns, and number of tracks measured.

tion zone between extended crust in west central Arizona and the Colorado Plateau, to mid-Tertiary magmatism that is prevalent in that region.

8. Thermal and Structural Implications

8.1. Overall Thermal History

[76] We can combine the AFT data from the Gold Butte block and the White Hills region to generate an overall AFT stratigraphy for the region and thus constrain the overall thermal and tectonic history for the western margin of the Colorado Plateau (Figure 13). This diagram shows that the Paleozoic and Mesozoic section of the Colorado Plateau was sufficiently thick to result in complete annealing of fission tracks in the Proterozoic basement beneath the Cambrian nonconformity [*Dumitru et al.*, 1994]. During and subsequent to burial, an apatite PAZ formed in the lower part of the sedimentary section (Grand Canyon region) and in the lower part of the sedimentary section and the upper part of the basement rocks under the nonconformity (western edge of the Colorado Plateau) before relatively rapid cooling associated with the Laramide orogeny marked by an increase in the slope of the profile (Figure 11). Track length distributions under the exhumed Laramide apatite PAZ do not indicate rapid cooling but rather a period of protracted Laramide cooling and later exposure to middle and/or late Tertiary heating induced by burial from Eocene sedimentary rocks (as discussed by *Dumitru et al.* [1994]). There is a remarkable similarity between the cooling/exhumation events we document in the South Virgin Mountains–White Hills and events documented by *Foster et al.* [1993] for core complexes and the transition zone in west central Arizona on the southwestern side of the Colorado Plateau. The regional extent and intensity of the late Eocene–Oligocene heating event (initiated ~35–30 Ma, as discussed in section 7.4) is not well constrained, although it is present both on the western and southwestern flanks of the Colorado Plateau.

[77] Note that the overall thermal history (Figure 13a) is constructed relative to the timing of events. If we correlate the different profiles relative to the lithostratigraphy (notably the sub-Cambrian nonconformity), we can place some constraints on the paleogeography (Figure 13b). AFT ages from basement directly under the Tapeats Sandstone (sub-Cambrian nonconformity) in the northern Gold Butte block are ~50 Ma with an apparent increase to the south of the block (Figure 4). On Garnet Mountain, AFT ages under the nonconformity are much older, 91–110 Ma (Figure 8) also reflecting an apparent southward trend toward older ages. This trend indicates that the level of the nonconformity shallowed to the south, as was previously noted with AFT thermochronology data [*Fitzgerald et al.*, 1991], indicating that the thickness of rock above the nonconformity prior to the mid-Miocene also decreased to the south, and that topography to the south was likely elevated. These relations

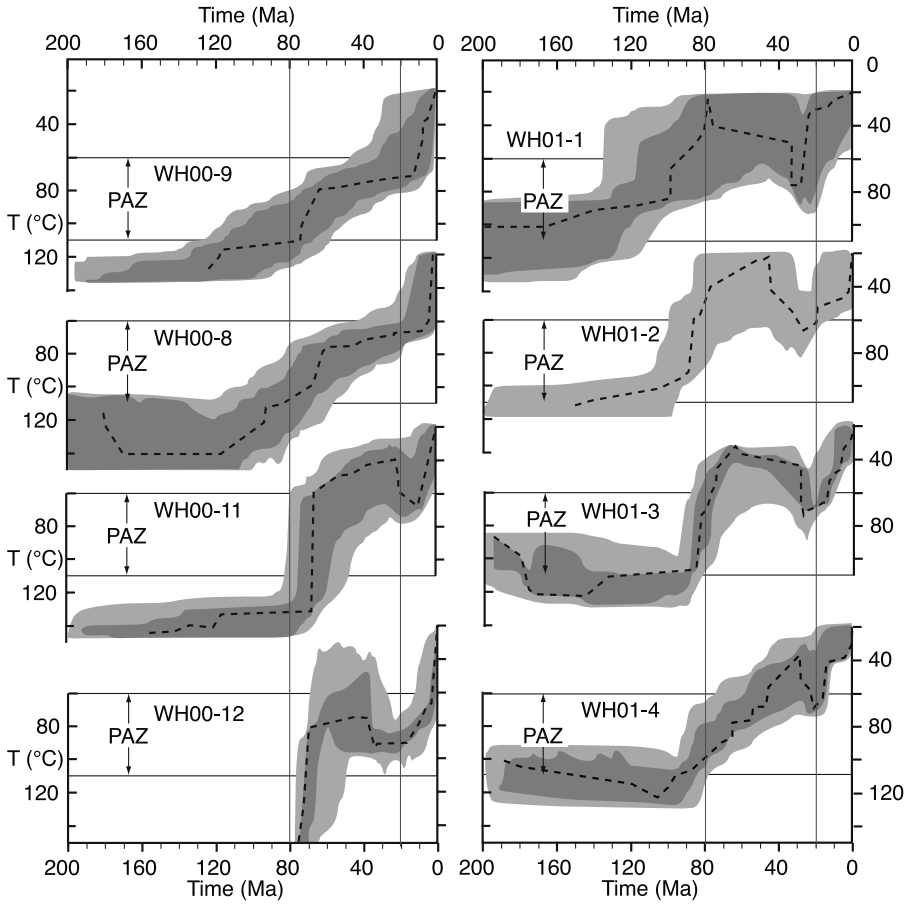

Figure 12. Temperature-time models for samples east of the Grand Wash fault, undertaken using HeFTy [*Ketcham*, 2005]. Samples are arranged according to relative crustal position as shown in Figure 11. Dark gray envelope is a "good fit" (i.e., the T-t path is supported by the data) and the light gray envelope an "acceptable fit" (i.e., the T-t path is not ruled out by the data). Model inputs are multiple T-t boxes with loose constraints designed to offer the opportunity for the model to explore Laramide cooling, Oligocene-Miocene reheating, and Miocene cooling; 10,000 paths were run in each model with model input including Dpar.

are compatible with the northward plunging Kingman arch, that was stripped of Phanerozoic strata by early to middle Tertiary erosion [*Bohannon*, 1984]. The northern margin of the arch was situated in the Lake Mead area. The distribution of late Cretaceous-Paleocene two-mica granites indicates that the arch plunged ~15° to the north in the White Hills area and accommodated more than 10 km of differential rock uplift between Gold Butte and the southern White Hills [*Faulds et al.*, 2001a]. Just to the east of the arch, in what is now the western Colorado Plateau, a gentle (<1–3°) northeastward tilt of strata also indicates a late Cretaceous–early Tertiary uplift to the south [e.g., *Peirce*, 1985].

[78] The Laramide break in slope (~75 Ma), indicative of the onset of more rapid cooling at the Grand Canyon [*Dumitru et al.*, 1994] and at Cedar Springs (Figures 8 and 11), is likewise at different stratigraphic levels and elevations (Figure 13b). In the Grand Canyon, the break in slope lies at ~1600 m elevation within the Paleozoic sedimentary rocks, and the nonconformity is at ~1050 m elevation. At Cedar Springs, the break in slope lies at ~1300 m and is found within the Proterozoic basement below the nonconformity at an elevation of ~1600 m. This indicates that prior to the onset of Laramide erosion, the thickness of the sedimentary rocks was ~300 m greater at the Grand Canyon than Cedar Springs (assuming similar upper crustal geothermal gradients just prior to 75 Ma).

8.2. Displacement Gradient

[79] The more or less synchronous extension documented in this study indicates the linkage of different fault segments along the SVWHD, with the southerly segments having a slower slip rate and therefore less displacement (Figure 14). Within the hanging wall of the SVWHD, the displacement gradient could be accommodated along (1) a few large, east striking, left-lateral faults, (2) many small-displacement, east striking, left-lateral faults, (3) anticlockwise vertical axis rotations (i.e., more distributed strain), or (4) some

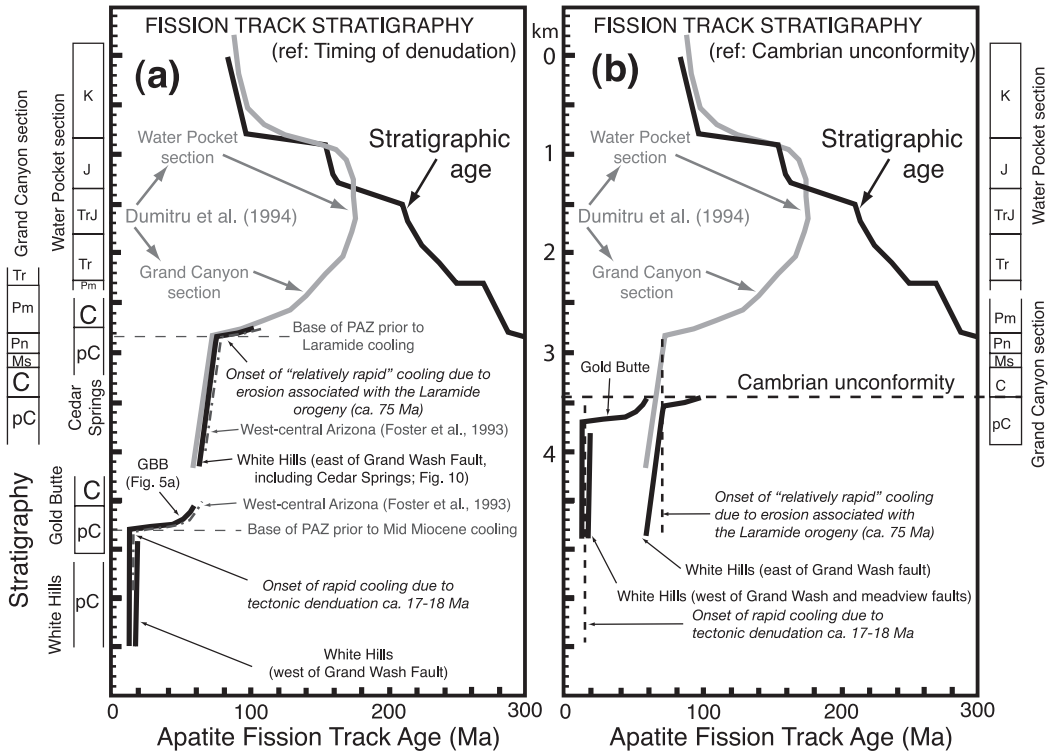

Figure 13. (a) Overall thermal history diagram that summarizes the cooling/denudation/tectonic history, constructed by creating the regional AFT stratigraphy. The stratigraphic column for each sampling region is diagrammatically shown on the left-hand side of the graph. Note that the different profiles are linked by timing of events rather than "true" stratigraphic or crustal level. Note the similarity in timing between denudation events between the White Hills–Gold Butte region on the western side of the Colorado Plateau and the AFT-derived thermal history from core complexes and the transition zone in west central Arizona on the southwestern side of the Colorado Plateau [*Foster et al.*, 1993]. (b) Overall thermal history diagram but with the different sampling regions linked by stratigraphic position (using the sub-Cambrian nonconformity as the reference). This diagram can be used to determine the relative crustal position of each region (see text for discussion). Note the stratigraphic thickness is from *Dumitru et al.* [1994] and is based on the thickness of units at the Grand Canyon and Water Pocket fold.

combination of the above. However, no large-displacement left-lateral faults have been documented in the hanging wall of the SVWHD. Also, paleomagnetic data [*Faulds et al.*, 2004] indicate no significant vertical axis rotation in SVWHD upper plate rocks, suggesting that movement on small-displacement, left-lateral faults accommodated differential slip on the SVWHD.

[80] The greater displacement along the Lakeside Mine fault in the Gold Butte block and penecontemporaneous initiation of extension there and in the White Hills indicate that the slip rate on the Lakeside Mine fault was more rapid than in the White Hills. This is important because the uncertainties in the slip rate for the Gold Butte block (8.6 ± 6 km/Ma) almost overlap at the 1σ level with the slip rates from the White Hills (weighted mean of 1.2 ± 0.7 km/Ma). Because the greatest difference between slip rates lies between the Gold Butte block and the northern White Hills, we postulate a transfer fault or series of faults, possibly buried beneath Lake Mead or postextensional deposits in the vicinity of Lake Mead, to accommodate the differential displacement.

[81] Farther south, near the latitude of Golden Rule Peak (Figures 2 and 8), several features suggest the presence of a transversely (i.e., east–west) oriented discontinuity that may mark a strain gradient between the Salt Spring and Cyclopic Mine segments. For example, a series of east striking left-lateral faults, west of the northern White Hills and along the trend of Golden Rule Peak, with ~5 km of cumulative slip may account for some of the displacement gradient [*Faulds et al.*, 2004]. The abrupt southward termination of a series of basalt-capped, east tilted fault blocks due west of Golden Rule Peak (Figures 2 and 8) may mark the presence of a buried fault. In addition, a 10 m wide, east striking cataclastic zone is present along the northern flank of Golden Rule Peak [*Ross-True*, 2008]; unfortunately, kinematic indicators were not recognized in this zone. Also,

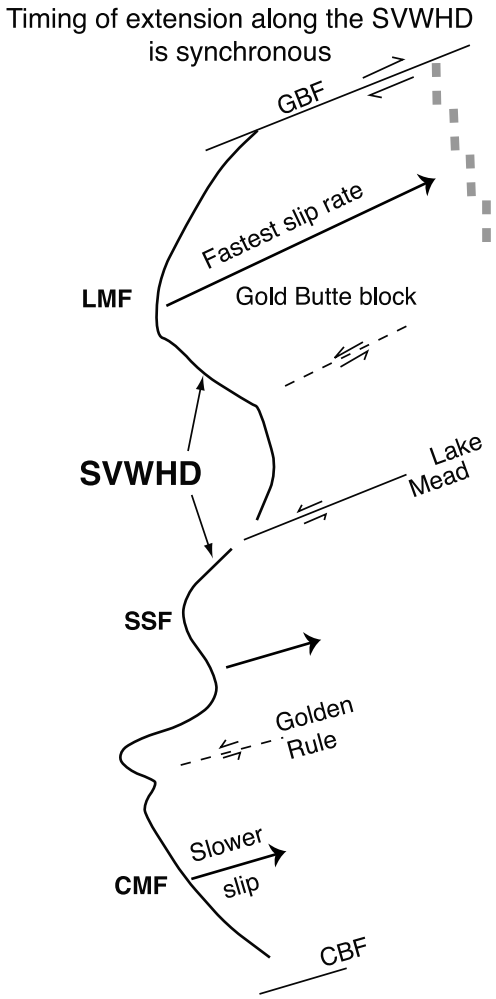

Figure 14. Conceptual diagram to explain the displacement gradient along the SVWHD. Present-day trace of the SVWHD is shown.

Golden Rule Peak is an anomalously oriented, east trending ridge in the footwall of the detachment that coincides with a high-amplitude (>300 m) short-wavelength corrugation that could have controlled the location of upper plate structures. Finally, the uniformly north striking, subvertical Paleoproterozoic foliations in the Lost Basin Range (footwall of the SVWHD) are sharply reoriented to west–northwest and east–northeast strikes along the eastward projection of the aforementioned features. This zone of anomalously oriented foliation, which also contains some east striking mylonite zones, raises the possibility that structures accommodating the displacement gradient in the upper plate may have been controlled by older, lower plate structures.

[82] The cause of the greater slip rates for the Gold Butte block area relative to areas to the south is uncertain. Greater fault displacement in the north has exposed deeper (mylonitic) rocks in the footwall of the Lakeside Mine fault. If the SVWHD is one continuous structure it follows that whereas the presence of brittle fault rocks in the south indicates less slip, it does not preclude slip from being accommodated on other structures. Extensive magmatism from ~19 to 13 Ma west of the White Hills (but not to the north of Lake Mead) (Figure 9) may have made the crust weaker preceding the onset of extension, facilitating accommodation of slip on a series of smaller faults in the White Hills. The lack of magmatism near the Gold Butte block just prior to the onset of extension may indicate that the Gold Butte crust was stronger and hence slip was accommodated along one major structure (Lakeside Mine fault). That the Gold Butte crust may have been cooler is supported by the 18–20°C/km preextension paleogeothermal gradient, whereas the preextension paleogeothermal gradient for the White Hills is not constrained, but could have been higher due to proximity to ~19–13 Ma volcanism in the northern Colorado River extensional corridor to the west of the White Hills.

9. Conclusions

[83] The main objective of this study was to constrain the origin of the displacement gradient along the SVWHD (deeper crustal levels in the north as compared to shallower crustal levels in the south) using AFT thermochronology. As such, this paper may serve as a case study on how to apply low-temperature thermochronology to similar extensional tectonic settings. The displacement gradient is manifested by the presence of mylonites along the Lakeside Mine fault in the Gold Butte block to the north where there has been ~17 km of slip versus cataclasites and brittle fault rocks in the White Hills to the south, where slip decreases to ~6 km. Samples were collected in a series of across-strike transects parallel to the extension direction and at along-strike intervals in the footwall of the detachment in order to constrain the timing of extension and rate of slip. The low-temperature thermochronology results indicate that tectonic exhumation associated with extension in the Gold Butte block was initiated at 17 Ma and that in the White Hills, extension was underway by ~18 Ma. A diachronous extension model, likely involving early extension in the north that propagated south, cannot explain the displacement gradient. The displacement gradient most likely resulted from synchronous along-strike exhumation and formation of the SVWHD by linkage of originally separate fault segments. Slip rates, constrained by the variation of AFT ages in rapidly cooled samples collected parallel to the extension direction, but not including samples across major structural features, suggest that slip along the Lakeside Mine fault was considerably more rapid in the Gold Butte block than in the White Hills region to the south. There, slip rates along the Salt Spring and Cyclopic Mine were much slower.

[84] We conclude that the displacement gradient along the SVWHD resulted from near-synchronous motion but with differential slip rates along different segments of the SVWHD. While one can conceptually envisage slip along the different segments as the result of rotation about a pole located to the south of the White Hills, it is more realistic

that different fault segments moved simultaneously and linked to form the SVWHD. Differential slip certainly seems to be required between the Gold Butte block and the northern White Hills, but it is uncertain how many east trending transverse structures there may be and how much differential slip was accommodated on each structure.

[85] By temporally linking AFT data from the Gold Butte block with data from the White Hills and the western edge of the Colorado Plateau, along with other published data, we can construct a composite AFT stratigraphic column to constrain the thermal history of the region. The thermal history reflects the transition of the Colorado Plateau as a depositional environment, through the Laramide orogeny and a poorly constrained heating event in the Oligocene, to the major cooling event associated with tectonic denudation and Miocene extension in the adjacent Basin and Range province. The marked contrast in AFT ages across some mapped faults in the region also indicates the previously unrecognized significance of some of these faults (e.g., Meadview fault).

[86] The Gold Butte block has proven to be a testing ground for thermochronologic methods and ways to use thermochronologic data in extended terranes. It is particularly notable because this is where the first exhumed PAZ (or PRZ) from a large tilt block in an extensional terrane was recognized, and where there are now four exhumed PAZ and PRZs from different methods, all exhibiting the same classic form [*Fitzgerald et al.*, 1991; *Reiners et al.*, 2000; *Bernet*, 2002; *Reiners*, 2005; this study], and all constraining the timing of the initiation of extension. As described, slip rate can be determined from the inverse slope of age versus horizontal distance for ages from samples collected, or projected, onto a line parallel to the extension direction. The restoration of easterly dipping sedimentary strata back to horizontal allows the original dip of the exhuming structure for the Gold Butte block, the Lakeside Mine fault, to be constrained at $\sim 60^\circ$. A new vector approach to constraining the dip of the exhuming fault is presented. While the uncertainties using this new approach in this example are large, the vector method does offer a potentially new avenue to constrain the dip of faults during their evolution, and in this case, the transition from a structure dipping $\sim 60^\circ$ to one that dips very gently. In this new vector approach, the angle between the vertical exhumation rate (constrained by the slope of the age versus paleodepth plot) and the slip rate on the fault (age versus horizontal) subtracted from 90° gives the dip of the fault as the rocks sampled cooled through the closure temperature of the thermochronometer being used.

[87] **Acknowledgments.** This study was supported by the National Science Foundation through funding to Fitzgerald (EAR-0002008), Duebendorfer (EAR-9909275 and EAR-0424900), and Faulds (EAR-9910977). Joan Fryxell is thanked for help in the field and early discussions. Discussions with Paul Umhoefer, Sue Beard, Nathan Blythe, and Zack Swaney helped clarify relations between the AFT data and the geology of the region. This is not to imply that they necessarily agree with the conclusions of this paper. Associate Editor Todd Ehlers, reviewer Dave Foster, and one anonymous reviewer are thanked for comments and reviews that helped improve this paper. Scott Miller is thanked for comments on the final version of this paper.

References

Anders, M. H., and R. W. Schlische (1994), Overlapping faults, intrabasin highs, and the growth of normal faults, *J. Geol.*, *102*, 165–180.

Anderson, R. E. (1973), Large magnitude late Tertiary strike-slip faulting north of Lake Mead, Nevada, *U.S. Geol. Surv. Prof. Pap., 794*, 18 pp.

Armstrong, P. A., T. A. Ehlers, D. S. Chapman, K. A. Farley, and P. J. J. Kamp (2003), Exhumation of the central Wasatch Mountains, Utah: 1. Patterns and timing of exhumation deduced from low-temperature thermochronology data, *J. Geophys. Res.*, *108*(B3), 2172, doi:10.1029/2001JB001708.

Armstrong, P. A., A. R. Taylor, and T. A. Ehlers (2004), Is the Wasatch fault (Utah, United States) segmented over million-year time scales?, *Geology*, *32*, 385–388, doi:10.1130/G20421.1.

Baldwin, S. L., and G. S. Lister (1998), Thermochronology of the South Cyclades Shear Zone, Ios, Greece: Effects of ductile shear in the argon partial retention zone, *J. Geophys. Res.*, *103*, 7315–7336.

Baldwin, S. L., G. S. Lister, E. J. Hill, D. A. Foster, and I. McDougall (1993), Thermochronologic constraints on the tectonic evolution of active metamorphic core complexes, D'Entrecasteaux Islands, Papua New Guinea, *Tectonics*, *12*, 611–628, doi:10.1029/93TC00235.

Beard, L. S. (1996), Paleogeography of the Horse Spring Formation in relation to the Lake Mead fault system, Virgin Mountains, Nevada and Arizona, in *Reconstructing the History of Basin and Range Extension Using Sedimentology and Stratigraphy*, edited by K. K. Bertatan, *Spec. Pap. Geol. Soc. Am.*, 303, 27–60.

Bernet, M. (2002), Exhuming the Alps though time; clues from detrital zircon fission-track ages, Ph.D. thesis, Yale Univ., New Haven, Conn.

Blacet, P. M. (1975), *Preliminary geologic map of the Garnet Mountain quadrangle, Mohave County*, Open File Report, United States Geological Survey, Arizona.

Blythe, N. (2005), Basin analysis associated with middle-Miocene detachment faulting, eastern Lake Mead region, northwest Arizona, M.S. thesis, 226 pp., North. Ariz. Univ., Flagstaff.

Bohannon, R. G. (1979), Strike-slip faults of the Lake Mead region of southern Nevada, *Cenozoic Paleogeography of the Western United States, Pacific Coast Paleogeography Symposium*, vol. 3, edited by J. M. Armentrout et al., pp. 129–139, Soc. of Econ. Paleontol. and Mineral., Pac. Sect., Los Angeles, Calif.

Bohannon, R. G. (1984), Nonmarine sedimentary rocks of Tertiary age in the Lake Mead region, southeastern Nevada and northwestern Arizona, *U.S. Geol. Surv. Prof. Pap., 1259*.

Brady, R. J. (2002), Very high slip rates on continental extension faults: New evidence from (U-Th)/He thermochronometry of the Buckskin Mountains, Arizona, *Earth Planet. Sci. Lett.*, *197*, 95–104, doi:10.1016/S0012-821X(02)00460-0.

Brady, R. J., B. Wernicke, and J. E. Fryxell (2000), Kinematic evolution of a large-offset continental normal fault system, South Virgin Mountains, Nevada, *Geol. Soc. Am. Bull.*, *112*, 1375–1397.

Brown, R. W. (1991), Backstacking apatite fission-track "stratigraphy": A method for resolving the erosional and isostatic rebound components of tectonic uplift histories, *Geology*, *19*, 74–77, doi:10.1130/0091-7613(1991)019<0074:BAFTSA>2.3.CO;2.

Carter, T. J., B. P. Kohn, D. A. Foster, and A. J. W. Gleadow (2004), How the Harcuvar Mountains metamorphic core complex became cool: Evidence from apatite (U-Th)/He thermochronology, *Geology*, *32*, 985–988, doi:10.1130/G20936.1.

Carter, T. J., B. P. Kohn, D. A. Foster, A. J. W. Gleadow, and J. D. Woodhead (2006), Late-stage evolution of the Chemehuevi and Sacramento detachment faults from apatite (U-Th)/He thermochronology—Evidence for mid-Miocene accelerated slip, *Geol. Soc. Am. Bull.*, *118*, 689–709, doi:10.1130/B25736.1.

Cascadden, T. E. (1991), Style of volcanism and extensional tectonics in the eastern Basin and Range province, northern Mohave County, Arizona, M.S. thesis, 156 pp., Univ. of Nev., Las Vegas.

Childs, C., J. Watterson, and J. J. Walsh (1995), Fault overlap zones within developing normal faults, *J. Geol. Soc.*, *152*, 535–549, doi:10.1144/gsjgs.152.3.0535.

Coven, B. (2005), Laramide shortening and Miocene extensional structures in the northeastern White Hills, Mohave County, Arizona, MS thesis, 113 pp., North. Ariz. Univ., Flagstaff.

Cowie, P. A., and C. H. Scholz (1992), Physical explanation for the displacement-length relationship of faults using a post-yield fracture mechanics model, *J. Struct. Geol.*, *14*, 1133–1148, doi:10.1016/0191-8141(92)90065-5.

dePolo, C. M., D. G. Clark, D. B. Slemmons, and A. R. Ramelli (1991), Historical surface faulting in the Basin and Range province, western North America: Implications for fault segmentation, *J. Struct. Geol.*, *13*, 123–136, doi:10.1016/0191-8141(91)90061-M.

Dickinson, W. R., M. A. Klute, M. J. Hayes, S. U. Janecke, E. R. Lundin, M. A. McKittrick, and M. D. Olivares (1988), Paleogeographic and paleotectonic setting of Laramide sedimentary basins in the central Rocky Mountain region, *Geol. Soc. Am. Bull.*, *100*, 1023–1039, doi:10.1130/0016-7606(1988)100<1023:PAPSOL>2.3.CO;2.

Donelick, R. A., P. B. O'Sullivan, and R. A. Ketcham (2005), Apatite fission track analysis, in *Low-Temperature Thermochronology: Techniques, Interpretations, and Applications*, *Rev. Mineral. Geochem.*, vol. 58, edited by P. W. Reiners and T. A. Ehlers, pp. 49–93, Mineral. Soc. of Am., Chantilly, Va.

Duebendorfer, E. M., and W. D. Sharp (1998), Variation in extensional strain along-strike of the South Virgin-White Hills detachment fault: Perspective from the northern White Hills, northwestern Arizona, *Geol. Soc. Am. Bull.*, *110*, 1574–1589, doi:10.1130/0016-7606(1998)110<1574:VIDASO>2.3.CO;2.

Duebendorfer, E. M., L. S. Beard, and E. I. Smith (1998), Restoration of Tertiary deformation in the Lake Mead region, southern Nevada, in *Accommodation Zones and Transfer Zones: The Regional Segmentation of the Basin and Range Province*, edited by J. Faulds and J. Stewart, *Spec. Pap. Geol. Soc. Am.*, 323, 127–148.

Duebendorfer, E. M., K. R. Chamberlain, and C. S. Jones (2001), Paleoproterozoic tectonic history of the Cerbat Mountains, northwestern Arizona; implications for crustal assembly in the southwestern United States, *Geol. Soc. Am. Bull.*, *113*, 575–590, doi:10.1130/0016-7606(2001)113<0575:PTHOTC>2.0.CO;2.

Dumitru, T. A. (1990), Subnormal Cenozoic geothermal gradients in the extinct Sierra Nevada magmatic arc: Consequences of Laramide and post-Laramide shallow-angle subduction, *J. Geophys. Res.*, *95*, 4925–4941, doi:10.1029/JB095iB04p04925.

Dumitru, T. A., P. B. Gans, D. A. Foster, and E. L. Miller (1991), Refrigeration of the western Cordilleran lithosphere during Laramide shallow-angle subduction, *Geology*, *19*, 1145–1148, doi:10.1130/0091-7613(1991)019<1145:ROTWCL>2.3.CO;2.

Dumitru, T. A., I. R. Duddy, and P. F. Green (1994), Mesozoic-Cenozoic burial, uplift, and erosion history of the west-central Colorado Plateau, *Geology*, *22*, 499–502, doi:10.1130/0091-7613(1994)022<0499:MCBUAE>2.3.CO;2.

Ehlers, T. A. (2005), Crustal thermal processes and the interpretation of thermochronometer data, in *Low-Temperature Thermochronology: Techniques, Interpretations, and Applications*, *Rev. Mineral. Geochem.*, vol. 58, edited by P. W. Reiners and T. A. Ehlers, pp. 315–350, Mineral. Soc. of Am., Chantilly, Va.

Ehlers, T. A., and D. S. Chapman (1999), Normal fault thermal regimes: Conducive and hydrothermal heat transfer surrounding the Wasatch fault, Utah, *Tectonophysics*, *312*, 217–234, doi:10.1016/S0040-1951(99)00203-6.

Ehlers, T. A., P. A. Armstrong, and D. S. Chapman (2001), Normal fault thermal regimes and the interpretation of low-temperature thermochronometers, *Phys. Earth Planet. Inter.*, *126*, 179–194, doi:10.1016/S0031-9201(01)00254-0.

Faulds, J. E., D. L. Feuerbach, M. K. Reagan, R. V. Metcalf, P. Gans, and J. D. Walker (1995), The Mt. Perkins block, northwestern Arizona: An exposed cross section of an evolving, preextensional to synextensional magmatic system, *J. Geophys. Res.*, *100*, 15,249–15,266, doi:10.1029/95JB01375.

Faulds, J. E., B. C. Schreiber, S. J. Reynolds, L. Gonzalez, and D. Okaya (1997), Origin and paleogeography of an immense, nonmarine Miocene salt deposit in the Basin and Range (western USA), *J. Geol.*, *105*, 19–36.

Faulds, J. E., E. I. Smith, and P. Gans (1999), Spatial and temporal patterns of magmatism and extension in the northern Colorado River extensional corridor, Nevada and Arizona: A preliminary report, guidebook, pp. 171–183, Nev. Pet. Soc., Reno.

Faulds, J. E., D. L. Feuerbach, C. F. Miller, and E. I. Smith (2001a), Cenozoic evolution of the northern Colorado River extensional corridor, southern Nevada and northwest Arizona, in *The Geologic Transition, High Plateaus to Great Basin—A Symposium and Field Guide, The Mackin Volume*, edited by M. C. Erskine et al., *Utah Geol. Assoc. Publ.*, 30, 239–271.

Faulds, J. E., L. M. Price, and M. A. Wallace (2001b), Pre-Colorado river paleogeography and extension along the Colorado Plateau-Basin and Range boundary, northwest Arizona, in *The Colorado River: Origin and Evolution*, edited by R. A. Young and E. E. Spamer, pp. 93–99, Grand Canyon Assoc., Grand Canyon, Ariz.

Faulds, J. E., E. M. Duebendorfer, R. T. Murphy, P. G. Fitzgerald, L. Peters, and W. C. McIntosh (2004), Implications of paleomagnetic data on displacement gradient accommodation along a major detachment fault, White Hills, northwest Arizona, *Geol. Soc. Am. Abstr. Programs*, *36*, 34.

Faulds, J. E., K. A. Howard, and E. M. Duebendorfer (2008), Cenozoic evolution of the abrupt Colorado Plateau-Basin and Range boundary, northwest Arizona: A tale of three basins, immense lacustrine-evaporite deposits, and the nascent Colorado River, in *Field Guide to Plutons, Volcanoes, Faults, Reefs, Dinosaurs and Possible Glaciation in Selected Areas of Arizona*, edited by E. M. Duebendorfer and E. I. Smith, pp. 115–151, Geol. Soc. of Am., Boulder, Colo.

Faulds, J. E., L. M. Price, L. W. Snee, and P. B. Gans (2009), A chronicle of Miocene extension near the Colorado Plateau-Basin and Range boundary, southern White Hills, northwestern Arizona: Paleogeographic and tectonic implications, in *Miocene Tectonics and Basin Development in the Lake Mead Region, Arizona and Nevada*, edited by P. Umhoefer, L. S. Beard, and L. Lamb, *Spec. Pap. Geol. Soc. Am.*, in press.

Fayon, A. K., S. M. Peacock, E. Stump, and S. J. Reynolds (2000), Fission track analysis of the footwall of the Catalina detachment fault, Arizona: Tectonic denudation, magmatism and erosion, *J. Geophys. Res.*, *105*, 11,047–11,062, doi:10.1029/1999JB900421.

Ferrill, D. A., J. A. Stamatakos, and D. Sims (1999), Normal fault corrugation: Implications for growth and seismicity of active normal faults, *J. Struct. Geol.*, *21*, 1027–1038, doi:10.1016/S0191-8141(99)00017-6.

Fitzgerald, P. G. (1992), The Transantarctic Mountains of southern Victoria Land: The application of apatite fission track analysis to a rift shoulder uplift, *Tectonics*, *11*, 634–662, doi:10.1029/91TC02495.

Fitzgerald, P. G. (1994), Thermochronologic constraints on post-Paleozoic tectonic evolution of the central Transantarctic Mountains, Antarctica, *Tectonics*, *13*, 818–836, doi:10.1029/94TC00595.

Fitzgerald, P. G. (2006), A new method to constrain fault dips using low-temperature thermochronology: An example from the Gold Butte block of southeastern Nevada, *Geol. Soc. Am. Abstr. Programs*, *38*, 416–417.

Fitzgerald, P. G., and A. J. W. Gleadow (1990), New approaches in fission track geochronology as a tectonic tool: Examples from the Transantarctic Mountains, *Nucl. Tracks*, *17*, 351–357.

Fitzgerald, P. G., J. E. Fryxell, and B. P. Wernicke (1991), Miocene crustal extension and uplift in southeastern Nevada: Constraints from apatite fission track analysis, *Geology*, *19*, 1013–1016, doi:10.1130/0091-7613(1991)019<1013:MCEAUI>2.3.CO;2.

Fitzgerald, P. G., S. J. Reynolds, E. Stump, D. A. Foster, and A. J. W. Gleadow (1994), Thermochronologic evidence for timing of denudation and rate of crustal extension of the South Mountains metamorphic core complex and Sierra Estrella, Arizona, *Nucl. Tracks*, *21*, 555–563.

Fitzgerald, P. G., R. B. Sorkhabi, T. F. Redfield, and E. Stump (1995), Uplift and denudation of the central Alaska Range: A case study in the use of apatite fission track thermochronology to determine absolute uplift parameters, *J. Geophys. Res.*, *100*, 20,175–20,191, doi:10.1029/95JB02150.

Fitzgerald, P. G., S. L. Baldwin, P. B. O'Sullivan, and L. E. Webb (2006), Interpretation of (U-Th)/He single grain ages from slowly cooled crustal terranes: A case study from the Transantarctic Mountains of southern Victoria Land, *Chem. Geol.*, *225*, 91–120, doi:10.1016/j.chemgeo.2005.09.001.

Flowers, R. M., B. P. Wernicke, and K. A. Farley (2008), Unroofing, incision, and uplift history of the southwestern Colorado Plateau from apatite (U-Th)/He thermochronometry, *Geol. Soc. Am. Bull.*, *120*, 571–587, doi:10.1130/B26231.1.

Foster, D. A., and A. J. W. Gleadow (1996), Structural framework and denudation history of the flanks Kenya and Anza rifts, East Africa, *Tectonics*, *15*, 258–271, doi:10.1029/95TC02744.

Foster, D. A., and E. B. John (1999), Quantifying tectonic exhumation in an extensional orogen with thermochronology: Examples from the southern Basin and Range province, in *Exhumation Processes: Normal Faulting, Ductile Flow and Erosion*, edited by U. Ring et al., *Geol. Soc. Spec. Publ.*, 154, 343–364.

Foster, D. A., D. S. Miller, and C. F. Miller (1991), Tertiary extension in the Old Womans Mountain area, California: Evidence from apatite fission track analysis, *Tectonics*, *10*, 875–886, doi:10.1029/91TC00865.

Foster, D. A., A. J. W. Gleadow, S. J. Reynolds, and P. G. Fitzgerald (1993), Denudation of metamorphic core complexes and the reconstruction of the transition zone, west central Arizona: Constraints from apatite fission track thermochronology, *J. Geophys. Res.*, *98*, 2167–2185, doi:10.1029/92JB02407.

Fryxell, J. E., and E. M. Duebendorfer (2005), Origin and trajectory of the Frenchman Mountain block, an extensional allochthon on the Basin and Range province, southern Nevada, *J. Geol.*, *113*, 355–371, doi:10.1086/428810.

Fryxell, J. E., G. G. Salton, J. Selverstone, and B. Wernicke (1992), Gold Butte crustal section, South Virgin Mountains, Nevada, *Tectonics*, *11*, 1099–1120, doi:10.1029/92TC00457.

Galbraith, R. F. (1981), On statistical models for fission track counts, *J. Int. Assoc. Math. Geol.*, *13*, 471–488, doi:10.1007/BF01034498.

Gleadow, A. J. W., and P. G. Fitzgerald (1987), Uplift history and structure of the Transantarctic Mountains: New evidence from fission track dating of basement apatites in the Dry Valleys area, southern Victoria Land, *Earth Planet. Sci. Lett.*, *82*, 1–14, doi:10.1016/0012-821X(87)90102-6.

Grasemann, B., and N. S. Mancktelow (1993), Two-dimensional thermal modelling of normal faulting: The Simplon Fault Zone, central Alps, Switzerland, *Tectonophysics*, *225*, 155–165, doi:10.1016/0040-1951(93)90277-Q.

Green, P. F. (1981), A new look at statistics in fission track dating, *Nucl. Tracks Radiat. Meas.*, *5*, 77–86.

Green, P. F. (1985), Comparison of zeta calibration baselines for fission-track dating of apatite, zircon and sphene, *Chem. Geol.*, *58*, 1–22, doi:10.1016/0168-9622(85)90023-5.

House, M. A., B. P. Wernicke, K. A. Farley, and T. A. Dumitru (1997), Cenozoic thermal evolution of the central Sierra Nevada, California, from (U-Th)/He thermochronometry, *Earth Planet. Sci. Lett.*, *151*, 167–179, doi:10.1016/S0012-821X(97)81846-8.

Howard, K. A., and D. A. Foster (1996), Thermal and unroofing history of a thick, tilted Basin and Range crustal section in the Tortilla Mountains, Arizona, *J. Geophys. Res.*, *101*, 511–522, doi:10.1029/95JB02909.

Howard, K. A., J. E. Faulds, L. S. Beard, and M. J. Kunk (2000), Reverse-drag folding across the path

of the antecedent early Pliocene Colorado River below the mouth of the Grand Canyon: Implications for plateau uplift, *Geol. Soc. Am. Abstr. Programs*, *32*, 41.

Hurford, A. J., and P. F. Green (1983), The zeta age calibration of fission track dating, *Isot. Geosci.*, *1*, 285–317.

John, B. E., and D. A. Foster (1993), Structural and thermal constraints on the initiation angle of detachment faulting in the southern Basin and Range: The Chemehuevi Mountains case study, *Geol. Soc. Am. Bull.*, *105*, 1091–1108, doi:10.1130/0016-7606(1993)105<1091:SATCOT>2.3.CO;2.

Kelleher, P. (2001), Structure in the lower plate of a major detachment, White Hills; Lake Mead, Arizona, M.S. thesis, 89 pp., North. Ariz. Univ., Flagstaff.

Ketcham, R. A. (1996), Distribution of heat-producing elements in the upper and middle crust of southern and west central Arizona: Evidence from the core complexes, *J. Geophys. Res.*, *101*, 13,611–13,632, doi:10.1029/96JB00664.

Ketcham, R. A. (2005), Forward and reverse modeling of low-temperature thermochronology data, in *Low-Temperature Thermochronology: Techniques, Interpretations, and Applications*, *Rev. Mineral. Geochem.*, vol. 58, edited by P. W. Reiners and T. A. Ehlers, pp. 275–314, Mineral. Soc. of Am., Chantilly, Va.

Kohn, B. P., and M. Eyal (1981), History of the crystalline basement of Sinai and its relation to opening of the Red Sea as revealed by fission track dating of apatites, *Earth Planet. Sci. Lett.*, *52*, 129–141, doi:10.1016/0012-821X(81)90215-6.

Laslett, G. M., A. J. W. Gleadow, and I. R. Duddy (1984), The relationship between fission track length and density in apatite, *Nucl. Tracks Radiat. Meas.*, *9*, 29–38, doi:10.1016/0735-245X(84)90019-X.

Lister, G. S., and S. L. Baldwin (1993), Plutonism and the origin of core complexes, *Geology*, *21*, 607–610, doi:10.1130/0091-7613(1993)021<0607:PATOOM>2.3.CO;2.

Lister, G. S., and G. A. Davis (1989), Models for the formation of metamorphic core complexes and mylonitic detachment terranes, *J. Struct. Geol.*, *11*, 65–94, doi:10.1016/0191-8141(89)90036-9.

Little, T. A., S. L. Baldwin, P. G. Fitzgerald, and B. M. Monteleone (2007), A young metamorphic core complex on Normanby Island, D'Entrecasteaux Islands, Papua New Guinea: Continental rifting processes near the Woodlark spreading ridge, *Tectonics*, *26*, TC1002, doi:10.1029/2005TC001911.

Longwell, C. R. (1936), Geology of the Boulder Reservoir floor, Arizona-Nevada, *Geol. Soc. Am. Bull.*, *47*, 1393–1476.

Lucchitta, I. (1966), Cenozoic Geology of the upper Lake Mead area adjacent to the Grand Wash Cliffs, Arizona, Ph.D. thesis, 218 pp., Penn. State Univ., University Park.

Lucchitta, I. (1972), Early history of the Colorado River in the Basin and Range province, *Geol. Soc. Am. Bull.*, *83*, 1933–1947, doi:10.1130/0016-7606(1972)83[1933:EHOTCR]2.0.CO;2.

Lucchitta, I., and R. A. Young (1986), Structure and geomorphic character of western Colorado Plateau in the Grand Canyon-Lake Mead region, in *Geology of Central and Northern Arizona*, guidebook, edited by J. D. Nations et al., pp. 159–176, Geol. Soc. of Am., Rocky Mt. Sect., Flagstaff, Ariz.

Matthews, J. (1976), Paleozoic stratigraphy and structural geology of the Wheeler Ridge area, northwestern Mojave County, Arizona, M.S. thesis, 144 pp., North. Ariz. Univ., Flagstaff.

McDougall, I., and T. M. Harrison (1999), *Geochronology and Thermochronology by the $^{40}Ar/^{39}Ar$ Method*, 2nd ed., Oxford Univ. Press, New York.

Myers, I. A., E. I. Smith, and R. V. Wyman (1986), Control of gold mineralization at the Cyclopic Mine, Gold Basin District, Mohave County, Arizona, *Econ. Geol.*, *81*, 1553–1557.

Naeser, C. W., B. Bryant, M. D. Crittenden, and M. L. Sorensen (1983), Fission-track ages of apatite in the Wasatch Mountains, Utah: An uplift study, in *Tectonic and Stratigraphic Studies in the Eastern Great Basin*, edited by D. M. Miller, *Mem. Geol. Soc. Am.*, 157, 29–36.

Nelson, S. T., J. P. Davidson, and K. R. Sullivan (1992), New age determinations of central Colorado Plateau laccoliths, Utah: Recognizing disturbed K-Ar systematics and re-evaluating tectonomagmatic relationships, *Geol. Soc. Am. Bull.*, *104*, 1547–1560, doi:10.1130/0016-7606(1992)104<1547:NADOCC>2.3.CO;2.

Peacock, D. C. P., and D. J. Sanderson (1991), Displacements, segment linkage, and relay ramps in normal fault zones, *J. Struct. Geol.*, *13*, 721–733, doi:10.1016/0191-8141(91)90033-F.

Peacock, D. C. P., and D. J. Sanderson (1994), Geometry and development of relay ramps in normal fault systems, *AAPG Bull.*, *78*, 147–165.

Peirce, H. W. (1985), Arizona's backbone: The transition zone, *Fieldnotes 15*, pp. 1–6, Ariz. Bur. of Geol. and Miner. Technol., Tucsco.

Price, L. M., and J. E. Faulds (1999), Structural development of a major segment of the Colorado Plateau-Basin and Range boundary, southern White Hills, Arizona, guidebook, pp. 139–170, Nev. Pet. Soc., Reno.

Reiners, P. W. (2002), (U-Th)/He chronometry experiences a renaissance, *Eos Trans. AGU*, *83*, 21, doi:10.1029/2002EO000012.

Reiners, P. W. (2005), Zircon (U-Th)/He thermochronometry, in *Low-Temperature Thermochronology: Techniques, Interpretations, and Applications*, *Rev. Mineral. Geochem.*, vol. 58, edited by P. W. Reiners and T. A. Ehlers, pp. 151–179, Mineral. Soc. of Am., Chantilly, Va.

Reiners, P. W., and M. T. Brandon (2006), Using thermochronology to understand orogenic erosion, *Annu. Rev. Earth Planet. Sci.*, *34*, 419–466, doi:10.1146/annurev.earth.34.031405.125202.

Reiners, P. W., R. Brady, K. A. Farley, J. E. Fryxell, B. Wernicke, and D. Lux (2000), Helium and argon thermochronometry of the Gold Butte Block, south Virgin Mountains, Nevada, *Earth Planet. Sci. Lett.*, *178*, 315–326, doi:10.1016/S0012-821X(00)00080-7.

Reiners, P. W., Z. Zhou, T. A. Ehlers, X. Changhai, M. T. Brandon, R. A. Donelick, and S. Nicolescu (2003), Post-progenic evolution of the Dabie Shan, eastern China, from (U-Th)/He and fission track thermochronology, *Am. J. Sci.*, *303*, 489–518, doi:10.2475/ajs.303.6.489.

Ross-True, K. L. (2008), Strain partitioning, segment linkage, and corrugation formation, South Virgin-White Hills detachment, northwestern Arizona, M.S. thesis, 96 pp., North. Ariz. Univ., Flagstaff.

Schlische, R. W., and M. H. Anders (1996), Stratigraphic effects and tectonic implications of the growth of normal faults and extensional basins, in *Reconstructing the History of Basin and Range Extension Using Sedimentology and Stratigraphy*, edited by K. K. Beratan, *Spec. Pap. Geol. Soc. Am.*, 303, 183–203.

Spencer, J. E. (1999), Geologic continuous casting below continental and deep-sea detachment faults and at the striated extrusion of Sacsayhuaman, Peru, *Geology*, *27*, 327–330, doi:10.1130/0091-7613(1999)027<0327:GCCBCA>2.3.CO;2.

Spencer, J. E., and S. J. Reynolds (1989), Middle Tertiary tectonics of Arizona and adjacent areas, in *Geologic Evolution of Arizona*, edited by J. P. Jenney and S. J. Reynolds, *Ariz. Geol. Soc. Dig.*, 17, 539–574.

Stewart, M. E., and W. J. Taylor (1996), Structural analysis and fault segment boundary identification along the Hurricane fault in southwestern Utah, *J. Struct. Geol.*, *18*, 1017–1029, doi:10.1016/0191-8141(96)00036-3.

Stockli, D. F. (2005), Application of low-temperature thermochronometry to extensional tectonic settings, in *Low-Temperature Thermochronology: Techniques, Interpretations, and Applications*, *Rev. Mineral. Geochem.*, vol. 58, edited by P. W. Reiners and T. A. Ehlers, pp. 411–448, Mineral. Soc. of Am., Chantilly, Va.

Stockli, D. F., K. A. Farley, and T. A. Dumitru (2000), Calibration of the apatite (U-Th)/He thermochronometer on an exhumed fault block, White Mountains, *Calif. Geol.*, *28*, 983–986.

Stockli, D. F., J. K. Linn, J. D. Walker, and T. A. Dumitru (2001), Miocene unroofing of the Canyon Range during extension along the Sevier Desert Detachment, west central Utah, *Tectonics*, *20*, 289–307, doi:10.1029/2000TC001237.

Stockli, D. F., B. E. Surpless, T. A. Dumitru, and K. A. Farley (2002), Thermochronological constraints on the timing and magnitude of Miocene and Pliocene extension in the central Wassuk Range, western Nevada, *Tectonics*, *21*(4), 1028, doi:10.1029/2001TC001295.

Stockli, D. F., S. Brichau, T. J. Dewane, C. Hager, and J. Schroeder (2006), Dynamics of large-magnitude extension in the Whipple Mountains metamorphic core complex, paper presented at 16th Annual Goldschmidt Conference, Eur. Assoc. of Geol., Melbourne, Australia, 27 Aug. to 1 Sept.

Swaney, Z. A. (2005), Tilting history of the Lost Basin Range and western Grand Wash trough, northwest Arizona: Regional implications, M.S. thesis, 144 pp., North. Ariz. Univ., Flagstaff.

ter Voorde, M., and G. Bertotti (1994), Thermal effects of normal faulting during rifted basin formation. 1. A finite difference model, *Tectonophysics*, *240*, 133–144, doi:10.1016/0040-1951(94)90268-2.

Theodore, T. G., W. N. Blair, and J. T. Nash (1987), Geology and gold mineralization of the Gold Basin-Lost Basin mining districts, Mohave County, Arizona, *U.S. Geol. Surv. Prof. Pap., 1361*, 167 pp.

Volborth, A. (1962), Rapakivi-type granites in the Precambrian complex of Gold Butte, Clark County, Nevada, *Geol. Soc. Am. Bull.*, *73*, 813–831, doi:10.1130/0016-7606(1962)73[813:RGITPC]2.0.CO;2.

Wallace, M. (1999), Cenozoic stratigraphic and structural framework of the southern Grand Wash trough, northwestern Arizona: Paleogeographic implications, M.S. thesis, 119 pp., Univ. of Iowa, Iowa City.

Wallace, M. W., J. E. Faulds, and R. J. Brady (2005), Geologic map of the Meadview North Quadrangle, Arizona and Nevada, Nev. Bur. of Mines and Geol., Las Vegas.

Wallace, R. E. (1984), Faulting related to the 1915 earthquakes in Pleasant Valley, Nevada, *U.S. Geol. Surv. Prof. Pap.*, *1274-A*, A1–A33.

Walsh, J. J., and J. Watterson (1988), Analysis of the relationship between displacements and dimensions of faults, *J. Struct. Geol.*, *10*, 239–247, doi:10.1016/0191-8141(88)90057-0.

Watterson, J. J. (1986), Fault dimensions; displacements and growth, *Pure Appl. Geophys.*, *124*, 365–373, doi:10.1007/BF00875732.

Wells, M. L., L. W. Snee, and A. E. Blythe (2000), Dating of major normal fault systems using thermochronology: An example from the Raft River detachment, Basin and Range, western United States, *J. Geophys. Res.*, *105*, 16,303–16,327, doi:10.1029/2000JB900094.

Wernicke, B. P. (1992), Cenozoic extensional tectonics of the U.S. Cordillera, in *The Geology of North America*, vol. G3, *The Cordilleran Orogen: Conterminous U.S.*, edited by B. C. Burchfiel et al., pp. 553–581, Geol. Soc. of Am., Boulder, Colo.

Wernicke, B., and G. J. Axen (1988), On the role of isostasy in the evolution of normal fault systems, *Geology*, *16*, 848–861, doi:10.1130/0091-7613(1988)016<0848:OTROII>2.3.CO;2.

Yin, A., and J. F. Dunn (1992), Structural and stratigraphic development of the Whipple-Chemehuevi detachment fault system, southeastern California; implications for the geometrical evolution of domal

and basinal low-angle normal faults, *Geol. Soc. Am. Bull.*, *104*, 659–674, doi:10.1130/0016-7606(1992)104<0659:SASDOT>2.3.CO;2.

Young, R. A. (1982), Paleogeomorphic evidence for the structural history of the Colorado Plateau margin in western Arizona, in *Mesozoic-Cenozoic Tectonic Evolution of the Colorado River Region, California, Arizona, and Nevada*, edited by E. G. Frost and D. M. Martin, pp. 29–39, Cordilleran Publ., San Diego, Calif.

Young, R. A., and W. J. Brennan (1974), The Peach Springs Tuff—Its bearing on structural evolution of the Colorado Plateau and development of Cenozoic drainage in Mohave County, Arizona, *Geol. Soc. Am. Bull.*, *85*, 83–90, doi:10.1130/0016-7606(1974)85<83:PSTIBO>2.0.CO;2.

Young, E. D., J. L. Anderson, H. S. Clarke, and W. M. Thomas (1989), Petrology of biotite-cordierite-garnet gneiss of the McCullough Range, Nevada 1: Evidence for Proterozoic low pressure fluid-absence granulite grade metamorphism in the southern Cordillera, *J. Petrol.*, *30*, 39–60.

E. M. Duebendorfer, Department of Geology, Northern Arizona University, Flagstaff, AZ 86011, USA.

J. E. Faulds, Nevada Bureau of Mines and Geology, University of Nevada at Reno, Reno, NV 89557, USA.

P. G. Fitzgerald, Department of Earth Sciences, Syracuse University, Syracuse, NY 13244, USA. (pgfitzge@syr.edu)

P. O'Sullivan, Apatite to Zircon Inc., 1075 Matson Road, Moscow, ID 83872-9709, USA.